Available online at www.sciencedirect.com
ScienceDirect
International Journal of Pharmaceutics 354 (2008) 49–55
INTERNATIONAL JOURNAL OF PHARMACEUTICS
www.elsevier.com/locate/ijpharm

Mini review

Effective gene delivery with novel liposomal bubbles and ultrasonic destruction technology

Ryo Suzuki [a], Tomoko Takizawa [a], Yoichi Negishi [b], Naoki Utoguchi [a], Kazuo Maruyama [a,*]

[a] *Department of Biopharmaceutics, School of Pharmaceutical Sciences, Teikyo University, 1091-1 Suwarashi, Sagamiko, Sagamihara, Kanagawa 229-0195, Japan*
[b] *School of Pharmacy, Tokyo University of Pharmacy and Life Science, Hachioji, Tokyo, Japan*

Received 28 July 2007; received in revised form 19 October 2007; accepted 22 October 2007
Available online 1 November 2007

Abstract

From the viewpoint of safety, non-viral vector systems represent an attractive gene delivery system for gene therapy. However, the transfection efficiency of non-viral vectors *in vivo* is generally very low. Previously, it was reported that microbubbles, utilized as imaging agents for diagnostic echocardiography, could promote gene delivery into cells when combined with ultrasound exposure. We therefore developed novel liposomal bubbles (Bubble liposomes) containing the lipid nanobubbles of perfluoropropane which is used as ultrasound imaging agent. These Bubble liposomes were smaller in diameter than conventional microbubbles and induced cavitation upon exposure to ultrasound. These results suggested that cavitation of these Bubble liposomes could be an efficient approach for delivering plasmid DNA into cells. In addition, in *in vivo* gene delivery, the combination of Bubble liposomes and ultrasound provided more effective gene delivery than conventional lipofection methods, further suggesting that Bubble liposomes could be effective as a non-viral vector system in *in vivo* gene delivery. In this review, we discuss the characteristics of Bubble liposomes and their potential utility as a gene delivery tool *in vitro* and *in vivo*.

Keywords: Gene delivery; Ultrasound; Cavitation; Bubbles; Liposomes

Contents

1. Introduction 49
2. Characteristics of Bubble liposomes 50
3. *In vitro* gene delivery with Bubble liposomes 51
4. *In vivo* gene delivery with Bubble liposomes 53
5. Conclusions 54
Acknowledgements 54
References 54

1. Introduction

Ultrasound has been successfully utilized in *in vivo* imaging, destruction of renal calculus, and treatment of fibroids in the uterus. It has been reported that ultrasound increases the permeability of the plasma membrane and reduces the thickness of the unstirred layer at the cell surface, thus facilitating the entry of DNA into cells (Fechheimer et al., 1987; Miller et al., 1996). The first studies investigating ultrasound for gene delivery used frequencies in the range of 20–50 kHz (Fechheimer et al., 1987; Joersbo and Brunstedt, 1990). However, these frequencies, along with cavitation, are also known to induce tissue damage if not properly controlled (Miller et al., 2002; Guzman et al., 2003; Wei et al., 2004). To address this problem, many gene deliv-

* Corresponding author. Tel.: +81 42 685 3722; fax: +81 42 685 3432.
E-mail address: maruyama@pharm.teikyo-u.ac.jp (K. Maruyama).

0378-5173/$ – see front matter © 2007 Elsevier B.V. All rights reserved.
doi:10.1016/j.ijpharm.2007.10.034

Table 1
Examples of microbubbles (Lindner, 2004)

Microbubble	Manufacturer	Shell	Gas	Mean size
Albunex	Molecular Biosystems	Albumin	Air	4.3 μm
Optison	Mallinckrodt/Amersham	Albumin	Octafluoropropane	2–4.5 μm
Definity	Bristol-Myers Squibb Medical Imaging	Lipid/surfactant	Octafluoropropane	1.1–3.3 μm
Imagent	Imcor	Lipid/surfactant	N_2/perfluorohexane vapor	6.0 μm
Sonovue	Bracco Diagnostics	Lipid	Sulfur hexafluoride	2–3 μm
Levovist	Schering AG	Lipid/galactose	Air	2–4 μm
Cardiosphere (BP127)	Point Biomedical	PLGA polymer/albumin	Nitrogen	4 μm
AI-700	Acusphere	PLGA polymer	Perfluorocarbon	2.2 μm
Sonovist	Schering AG	Cyanoacrylate polymer	Air	
Sonazoid	GE Healthcare	Lipid (single layer)	Perfluorocarbon	3 μm
Bubble liposomes		Lipid (bilayer)	Perfluorocarbon	950 nm

PLGA: polylactide-*co*-glycolide.

ery studies have been conducted using therapeutic ultrasound, which operates at frequencies of 1–3 MHz and at intensities of 0.5–2.5 W/cm^2 (Kim et al., 1996; Tata et al., 1997; Duvshani-Eshet and Machluf, 2005). In addition, it has been reported that the combination of therapeutic ultrasound and microbubble echo contrast agents enhances gene transfection efficiency (Greenleaf et al., 1998; Shohet et al., 2000; Taniyama et al., 2002a,b; Li et al., 2003; Chen et al., 2006; Sonoda et al., 2006; Suzuki et al., 2007a,b, in press). Using this approach, DNA is effectively and directly transferred into the cytosol. Conventional microbubbles encapsulating ultrasound contrast agents, based on protein microspheres and sugar microbubbles, are commercially available; the diameters of these bubbles are between 1 and 6 μm (Table 1) (Lindner, 2004). However, although the mean diameter of, for example, Optison microbubbles is about 2.0–4.5 μm, bubbles of up to 32 μm in diameter are present in the preparation, suggesting that Optison is too large to reach peripheral tissues. Tsunoda et al. (2005) reported that several mice died immediately after i.v. injection of Optison, without ultrasound exposure, due to lethal embolisms in vital organs. The same problem has not been reported in humans, but the possibility exists that Optison cannot pass through capillary vessels. Therefore, microbubbles should generally be smaller than red blood cells, necessitating the development of novel bubbles which are smaller than conventional microbubbles.

Liposomes have several advantages as drug, antigen and gene delivery carriers (Maruyama et al., 1990, 2004; Ishida et al., 2001; Harata et al., 2004; Yanagie et al., 2004; Hatakeyama et al., 2007; Kawamura et al., 2006; Yanagie et al., 2006). For example, their size can be easily controlled, and they can be modified to incorporate a targeting function. Using liposome technology, it was expected that these novel bubbles would be smaller than conventional microbubbles. Thus, we attempted to develop novel liposomal bubbles containing the ultrasound imaging gas, perfluoropropane. And we have successfully developed liposomal bubbles in which the lipid nanobubbles of perfluoropropane with lipids derived from liposomes were encapsulated. We called these bubbles "Bubble liposomes", and confirmed that Bubble liposomes are smaller than Optison. In addition, 1 mg of Bubble liposomes (in terms of lipid amount) injected into the tail veins of mice did not result in any deaths, indicating that these novel liposomes might be safe for use *in vivo*. Moreover, we reported that Bubble liposomes could be used as a novel non-viral gene delivery tool by combining the bubbles with ultrasound exposure (Suzuki et al., 2007a,b, in press). The present review focuses on gene delivery systems utilizing Bubble liposomes in combination with ultrasound.

2. Characteristics of Bubble liposomes

Bubble liposomes are polyethyleneglycol-modified liposomes (PEG-liposomes) prepared by the reverse phase evaporation method. PEG-liposomes were placed in vials supercharged with perfluoropropane gas, then sonicated in a bath sonicator. The suspension of Bubble liposomes became cloudier than the original liposome suspension (Fig. 1(a) and (b)). Observation of both Bubble liposomes and Optison under a microscope equipped with a darklite illuminator (NEPA Gene Co. Ltd., Chiba, Japan) (Fig. 1(c) and (d)) showed that Bubble liposomes are smaller than Optison. The diameter of most Bubble liposomes is less than 2 μm, and the average diameter is about 950 nm (Suzuki et al., in press). In addition, we confirmed by means of transmission electron microscopy that perfluoropropane gas was in fact trapped within the Bubble liposomes (Fig. 1(e)). Interestingly, there were nanobubbles in the lipid bilayer, suggesting that Bubble liposomes differ from conventional microbubbles, in which an echo gas is encased by a lipid monolayer (Fig. 1(f)). Kodama et al. and Klibanov et al. described microbubbles prepared from distearoylphospatidylcholine and PEG-stearate (Leong-Poi et al., 2003; Takahashi et al., 2007). At the same time, perfluoropropane was entrapped within lipid micelles composed of DSPC and DSPE-PEG (2k), forming nanobubbles. These nanobubbles were encapsulated within the reconstituted liposomes, which were approximately 1 μm in diameter rather than the 150–200 nm of the original liposomes (Suzuki et al., in press). These Bubble liposomes were too large to use to passively target tumor tissues by the enhanced permeability and retention (EPR) effect. However, we expected that Bubble liposomes could penetrate tissues deeper than conventional microbubbles by means of blood circulating in organs.

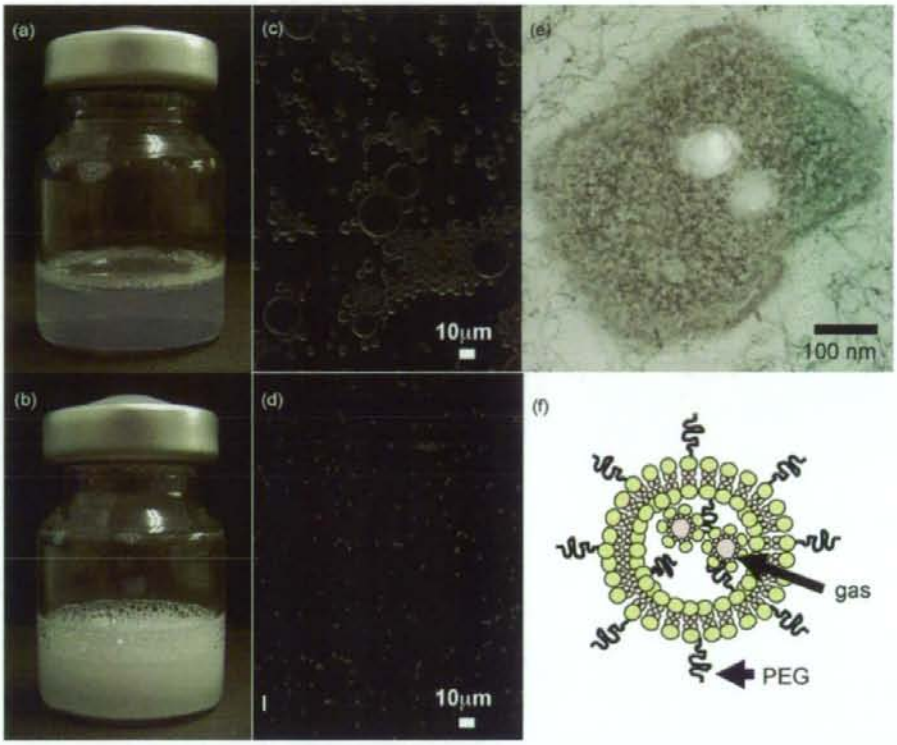

Fig. 1. Structure of Bubble liposomes. PEG-liposomes (a) were sonicated with supercharged perfluoropropane gas, generating Bubble liposomes (b). Optison (c) and Bubble liposomes (d) were observed with a microscope using a darklite illuminator. (e) Transmission electron microscopy (TEM) of Bubble liposomes. (f) Scheme showing the structure of Bubble liposomes.

To confirm the gas trapped in Bubble liposomes, we observed Bubble liposomes using ultrasound imaging (UF-750XT, Fukuda Denshi Co Ltd., Tokyo, Japan) as shown in Fig. 2(a). Echo signals were apparently enhanced in Bubble liposomes compared with conventional PEG-liposomes (Fig. 2(b) and (c)). Therefore, it is expected that Bubble liposomes can be utilized as ultrasound imaging agents, and indeed we succeeded in conducting echocardiography using Bubble liposomes (Suzuki et al., 2007b).

Conventional microbubbles can induce cavitation upon exposure to ultrasound (Tachibana and Tachibana, 1995). Cavitation supplies the energy required to deliver extracellular molecules into the cytosol (Taniyama et al., 2002a,b; Kinoshita and Hynynen, 2005a,b; Larina et al., 2005). We confirmed whether Bubble liposomes could induce cavitation by exposing Bubble liposomes to ultrasound generated using a Sonoporation Gene Transfection System (Sonopore, NEPA Gene Co. Ltd., Chiba, Japan). After ultrasound exposure, the strength of the ultrasound echo signals decreased markedly upon ultrasound imaging compared with Bubble liposomes not exposed to ultrasound (Fig. 2(d) and (e)). This result indicated that cavitation was effectively induced by the combination of Bubble liposomes and ultrasound exposure, suggesting that Bubble liposomes could be utilized as a gene delivery tool.

3. *In vitro* gene delivery with Bubble liposomes

Gene transfection by means of microbubbles has been previously reported (Taniyama et al., 2002a,b; Li et al., 2003; Chen et al., 2006; Sonoda et al., 2006). Li et al. (2003) compared the gene transfection efficiency of Albunex, Optison and Levovist into skeletal muscle cells and found that the efficiency of Optison was the highest. In addition, Machluf et al. reported enhanced transfection efficiency into kidney cells using a combination of Optison and ultrasound (Duvshani-Eshet et al., 2006). Under these conditions, cell surfaces became rougher, and showed depressions with diameters of 100–300 nm. Also using Optison in combination with ultrasound, Taniyama et al. (2002a,b) investigated transfection into vascular endothelial cells and smooth muscle cells. They reported small holes in the cells immediately following ultrasound exposure with Optison, but the holes disappeared after 24 h. Most gene delivery studies using microbubbles utilize commercially available microbubbles such as Optison; there are few reports regarding gene transfection with liposomal bubbles. Therefore, we examined the transduction of naked plasmid DNA into COS-7 cells by Bubble liposomes and/or ultrasound. Levels of luciferase expression were much higher after ultrasound treatment in the presence of Bubble liposomes compared to in their absence (Fig. 3). Interestingly, gene expres-

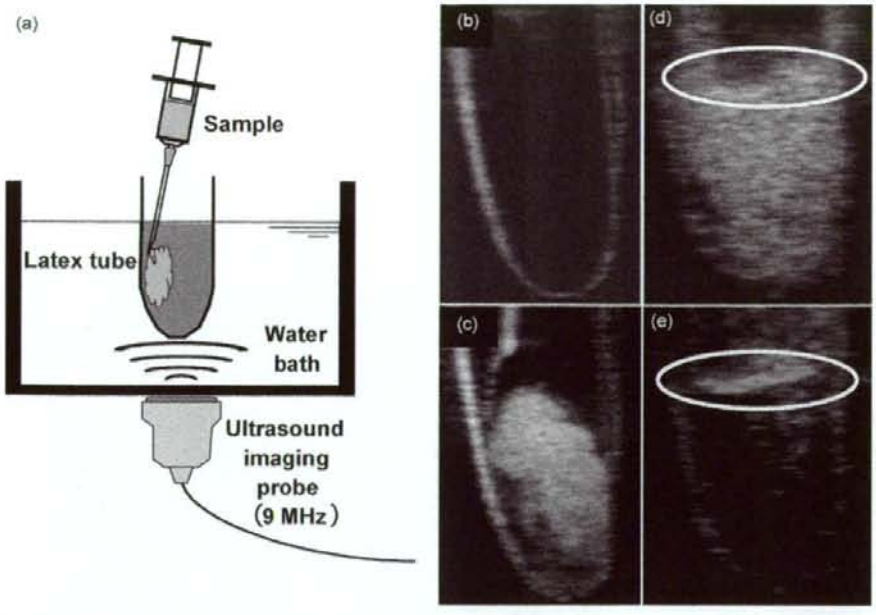

Fig. 2. Ultrasonography of Bubble liposomes. The ultrasonography method for observing Bubble liposomes is shown in (a). PEG-liposomes (b) or Bubble liposomes (c) were injected into a PBS-filled latex tube in a water bath and the samples were observed with ultrasonography. To confirm the disruption of the Bubble liposomes, the Bubble liposomes were observed with ultrasonography before (d) and after (e) ultrasound exposure (2 MHz, 2.5 W/cm^2, 10 s).

sion efficiency was very high following ultrasound exposures as short as 10 s. We also confirmed that Bubble liposomes could effectively deliver plasmid DNA into cells even after 1 s of ultrasound exposure (Suzuki et al., in press). Thus, Bubble liposomes are novel gene delivery agents that can almost instantaneously transfect extracellular plasmid DNA into cells.

Heat and jet streams are generally induced by cavitation, which might damage cells. We therefore examined the effects of ultrasound on cells both in the presence and absence of Bubble liposomes (Fig. 4). Cell viability was measured using the MTT assay (Mosmann, 1983) at 1 day following treatment. Ultrasound did not damage COS-7 cells in the absence of Bubble liposomes, and only slightly affected the cells even when

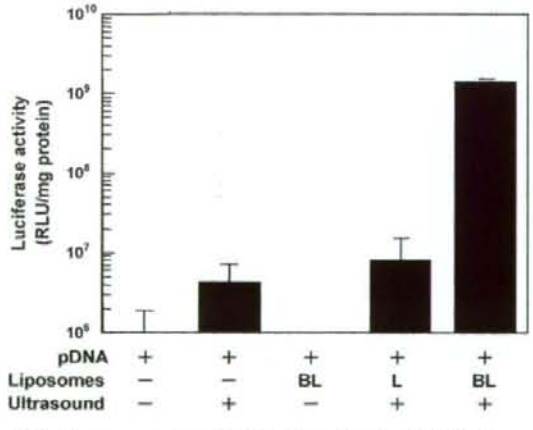

Fig. 3. Luciferase expression in COS-7 cells transfected with Bubble liposomes following ultrasound exposure. COS-7 cells (1×10^5 cells/500 μL per tube) were mixed with pCMV-Luc (5 μg) and Bubble liposomes (60 μg). The cell mixture was exposed to ultrasound (frequency: 2 MHz; duty: 50%; burst rate: 2 Hz; intensity: 2.5 W/cm^2; time: 10 s). The cells were washed and cultured for 2 days, then luciferase activity was measured. Each data point represents the mean ± S.D. ($n = 3$). BL: Bubble liposomes; L: PEG-liposomes.

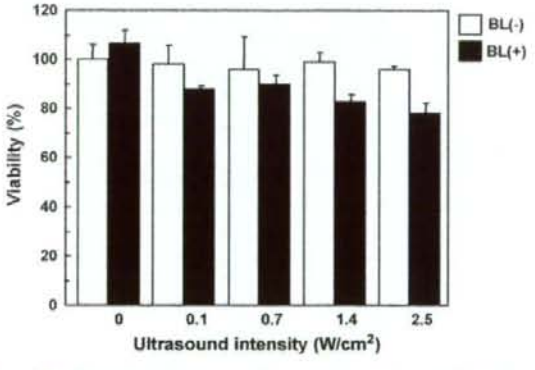

Fig. 4. Viability of COS-7 cells exposed to ultrasound and Bubble liposomes. COS-7 cells were exposed to each ultrasound intensity with or without Bubble liposomes, then the cells were cultured for 24 h and their viability was assessed using the MTT assay. Briefly, MTT (5 mg/mL, 10 μL) was added to each well and the cells were incubated at 37 °C for 4 h. The formazan product was dissolved in 100 μL of 10% sodium dodecyl sulfate (SDS) containing 15 mM HCl. Color intensity was measured using a microplate reader at test and reference wavelengths of 595 and 655 nm, respectively. Each data point represents the mean ± S.D. ($n = 3$). BL: Bubble liposomes.

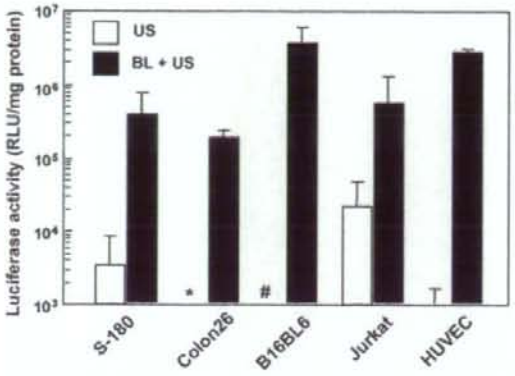

Fig. 5. Luciferase expression in various cell types transfected using Bubble liposomes and ultrasound. Cells (1×10^5 cells/500 μL per tube) were mixed with pCMV-Luc (5 μg) and Bubble liposomes (60 μg). A portion of the cell mixture was exposed to ultrasound (frequency: 2 MHz; duty: 50%; burst rate: 2 Hz; intensity: 2.5 W/cm^2; time: 10 s). Exposed and non-exposed cells were washed and cultured for 2 days, then luciferase activity was measured. Each data point represents the mean ± S.D. ($n = 3$). BL: Bubble liposomes; US: ultrasound. *<10^3 RLU/mg protein, #<10^6 RLU/mg protein.

the amount of ultrasound administered was sufficient to induce cavitation of the Bubble liposomes. We also confirmed that the cavitation induced with Bubble liposomes did not damage plasmid DNA (Suzuki et al., 2007a). In addition, we assessed the feasibility of delivering genes into various types of cells such as mouse tumor cells, a human T cell line and human vessel endothelial cells. Fig. 5 shows that Bubble liposomes combined with ultrasound more effectively delivered plasmid DNA into all these cell types than did ultrasound alone. *In vivo* gene delivery with Bubble liposomes requires the delivery of plasmid DNA into cells in the presence of serum. Thus, we examined the effect of serum on gene delivery with Bubble liposomes (Fig. 6) and showed that gene expression following treatment

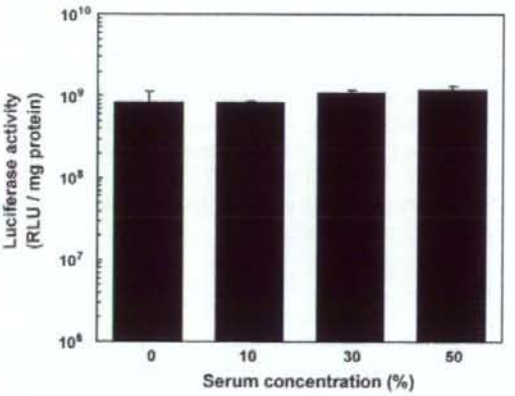

Fig. 6. Effect of serum on transfection efficiency of Bubble liposomes. COS-7 cells (1×10^5 cells/500 μL) mixed with pCMV-Luc (0.25 μg) and Bubble liposomes (60 μg) were exposed to ultrasound (frequency: 2 MHz; duty: 50%; burst rate: 2 Hz; intensity: 2.5 W/cm^2; time: 10 s) in the absence or presence of serum (0, 10, 30 and 50%). The cells were washed and cultured for 2 days, then luciferase activity was measured. Data are shown as means ± S.D. ($n = 3$).

with Bubble liposomes was not affected even in the presence of serum.

4. *In vivo* gene delivery with Bubble liposomes

To further assess the potential of *in vivo* gene delivery using Bubble liposomes and ultrasound, the delivery of plasmid DNA into the femoral artery of mice was studied (Fig. 7). Bubble liposomes and plasmid DNA were injected into the femoral artery as ultrasound was transdermally applied downstream of the injection site. Additionally, using Lipofectamine 2000, gene expression efficiency using Bubble liposomes was compared to conventional lipofection (Fig. 7(a)). The combination of Bubble liposomes and ultrasound exposure was more effective than conventional lipofection in inducing gene expression in the femoral artery. Moreover, gene expression with Bubble liposomes and ultrasound exposure was observed only in the area exposed to ultrasound (Fig. 7(b)). These results suggest that Bubble liposomes quickly deliver plasmid DNA into the artery by cavitation even after only short contact between the Bubble liposomes and endothelial cells by means of the blood stream. It had been thought that plasmid DNA was delivered into endothelial cells lining the femoral artery because it was physiologically difficult for plasmid DNA and Bubble liposomes to extravasate from a normal artery. Mizuguchi et al. (1998) reported effective cancer gene therapy by locally introducing cytokine genes by gene delivery into arteries leading to the tumor, or delivery into arteries in the tumor tissue. Therefore, we anticipated that Bubble liposomes could be used to deliver genes into arteries in tumor tissue. In the footpad tumor bearing mouse model, Bubble liposomes and luciferase-encoding plasmid DNA were injected into arteries leading to the tumor while the tumor tissue was transdermally exposed to ultrasound. After 2 days, luciferase expression was observed only in the tumor tissue. In addition, the gene expression efficiency of this method was higher than that of the conventional lipofection method using Lipofectamine 2000 (Suzuki et al., in press). We therefore believe that this method has significant advantages for tumor gene therapy using non-viral vectors.

In another study, we compared transfection efficiency using Bubble liposomes and Optison. Green fluorescent protein (GFP)-encoding plasmid DNA was delivered into cultured rabbit corneal epithelial cells using ultrasound exposure in the presence of Bubble liposomes or Optison. Gene expression efficiency with Bubble liposomes vs. Optison was about 25 and 10%, respectively. In an *in vivo* study, GFP-encoding plasmid DNA was injected into rat subconjunctiva tissue using bubbles and ultrasound exposure. Bubble liposomes more effectively induced gene expression in the tissue compared with Optison (Yamashita et al., in press). These results show that Bubble liposomes are more effective than conventional microbubbles at delivering genes for ophthalmologic treatments.

It is believed that gene expression using Bubble liposomes is transient, and that in order to maintain extended gene expression it is necessary to inject the liposomes repeatedly. However, there are reports of accelerated blood clearance (ABC) of PEGylated liposomes after repeat injections due to the enhanced accumu-

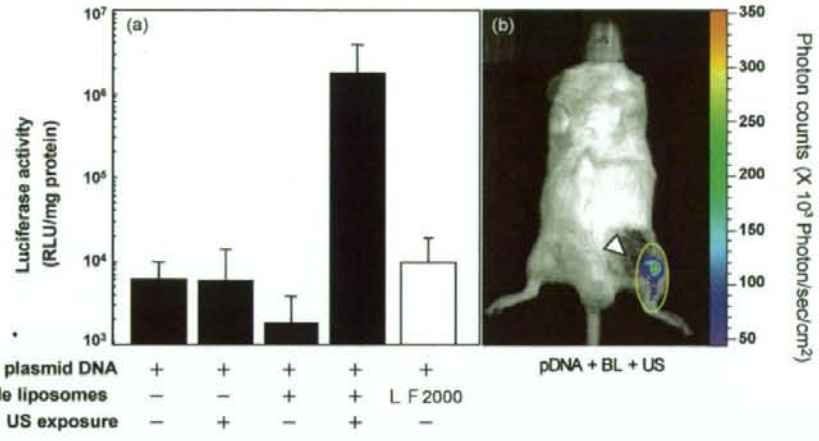

Fig. 7. Gene delivery to mouse femoral artery using Bubble liposomes. Each sample containing plasmid DNA (10 μg) was injected into the mouse femoral artery while ultrasound (frequency: 1 MHz; duty: 50%; burst rate: 2 Hz; intensity: 1 W/cm^2; time: 2 min) was applied downstream of the injection site. (a) Luciferase expression in the area of the femoral artery exposed to ultrasound 2 days after transfection. Data are shown as mean ± S.D. ($n = 5$). (b) *In vivo* luciferase imaging 2 days after transfection of mice treated with plasmid DNA, Bubble liposomes and ultrasound exposure. The photon counts are indicated by the pseudo-color scales. The arrowhead shows the injection site and the circle shows the ultrasound exposure area. BL: Bubble liposomes; LF 2000: Lipofectamine 2000; US: ultrasound.

lation of PEGylated liposomes in the liver and thus its rapid clearance from blood circulation. Ishida et al. reported that IgM secreted in response to the first dose is involved in this clearance response (Ishida et al., 2006; Wang et al., 2007). In *in vivo* gene delivery using Bubble liposomes and ultrasound exposure, ultrasound is normally applied at the same time as the Bubble liposomes are injected, or soon after the injection. Bubble liposomes would therefore immediately deliver plasmid DNA into the cells upon ultrasound exposure *in vivo*. Therefore, it is thought that transfection efficiency will not be affected by the ABC phenomenon even in the presence of IgM against PEGylated liposomes after multiple injections, and that repeat injections of Bubble liposomes will not reduce the efficiency of gene delivery *in vivo*.

5. Conclusions

We prepared Bubble liposomes containing submicron-sized bubbles using a novel methodology. These novel liposomes induced cavitation upon exposure to ultrasound, which resulted in plasmid DNA transduction into cells both *in vitro* and *in vivo*. Gene delivery was complete within a very short period of time. Therefore, Bubble liposomes could effectively deliver plasmid DNA into an artery *in vivo*, even in the blood stream. In this study, a mixture of plasmid DNA and Bubble liposomes was injected into the femoral artery. Interestingly, the area of gene uptake using Bubble liposomes was limited to the area exposed to ultrasound, indicating that gene expression depends on the area exposed to ultrasound. Therefore, gene targeting should be easily achieved using this gene delivery system simply by changing the site of ultrasound exposure. Our future goal is to establish non-invasive and tissue-specific gene delivery with Bubble liposomes after systemic injection.

Acknowledgements

We are grateful to Dr. Katsuro Tachibana (Department of Anatomy, School of Medicine, Fukuoka University) for technical advice regarding the induction of cavitation with ultrasound, to Ms. Kumiko Tanaka, Ms. Kaori Sawamura, Mr. Yusuke Oda, Mr. Eisuke Namai, Mr. Yuta Saito, Ms. Naoko Yamashita and Mr. Yosuke Suyama (Department of Biopharmaceutics, School of Pharmaceutical Sciences, Teikyo University) for excellent technical assistance, to Dr. Yoshio Nakano and Dr. Akinori Suginaka (NOF Corporation) for technical advice regarding lipids and for providing the lipids, and to Mr. Yasuhiko Hayakawa, Mr. Takahiro Yamauchi and Mr. Kosho Suzuki (NEPA Gene Co. Ltd.) for technical advice regarding ultrasound exposure.

This study was supported by an Industrial Technology Research grant (04A05010) in 2004 from the New Energy and Industrial Technology Development Organization (NEDO) of Japan, a Grant-in-Aid for the Encouragement of Young Scientists (160700392), an Exploratory Research grant (16650126) from the Japan Society for the Promotion of Science, and a Research on Advanced Medical Technology in Health and Labour Sciences Research grant (17070301) from the Ministry of Health, Labour and Welfare.

References

Chen, S., Ding, J.H., Bekeredjian, R., Yang, B.Z., Shohet, R.V., Johnston, S.A., Hohmeier, H.E., Newgard, C.B., Grayburn, P.A., 2006. Efficient gene delivery to pancreatic islets with ultrasonic microbubble destruction technology. Proc. Natl. Acad. Sci. U.S.A. 103, 8469–8474.

Duvshani-Eshet, M., Machluf, M., 2005. Therapeutic ultrasound optimization for gene delivery: a key factor achieving nuclear DNA localization. J. Control. Rel. 108, 513–528.

Duvshani-Eshet, M., Adam, D., Machluf, M., 2006. The effects of albumin-coated microbubbles in DNA delivery mediated by therapeutic ultrasound. J. Control. Rel. 112, 156–166.

Fechheimer, M., Boylan, J.F., Parker, S., Sisken, J.E., Patel, G.L., Zimmer, S.G., 1987. Transfection of mammalian cells with plasmid DNA by scrape loading and sonication loading. Proc. Natl. Acad. Sci. U.S.A. 84, 8463–8467.

Greenleaf, W.J., Bolander, M.E., Sarkar, G., Goldring, M.B., Greenleaf, J.F., 1998. Artificial cavitation nuclei significantly enhance acoustically induced cell transfection. Ultrasound Med. Biol. 24, 587–595.

Guzman, H.R., McNamara, A.J., Nguyen, D.X., Prausnitz, M.R., 2003. Bioeffects caused by changes in acoustic cavitation bubble density and cell concentration: a unified explanation based on cell-to-bubble ratio and blast radius. Ultrasound Med. Biol. 29, 1211–1222.

Harata, M., Soda, Y., Tani, K., Ooi, J., Takizawa, T., Chen, M., Bai, Y., Izawa, K., Kobayashi, S., Tomonari, A., Nagamura, F., Takahashi, S., Uchimaru, K., Iseki, T., Tsuji, T., Takahashi, T.A., Sugita, K., Nakazawa, S., Tojo, A., Maruyama, K., Asano, S., 2004. CD19-targeting liposomes containing imatinib efficiently kill Philadelphia chromosome-positive acute lymphoblastic leukemia cells. Blood 104, 1442–1449.

Hatakeyama, H., Akita, H., Kogure, K., Oishi, M., Nagasaki, Y., Kihira, Y., Ueno, M., Kobayashi, H., Kikuchi, H., Harashima, H., 2007. Development of a novel systemic gene delivery system for cancer therapy with a tumor-specific cleavable PEG-lipid. Gene Ther. 342, 194–200.

Ishida, O., Maruyama, K., Tanahashi, H., Iwatsuru, M., Sasaki, K., Eriguchi, M., Yanagie, H., 2001. Liposomes bearing polyethyleneglycol-coupled transferrin with intracellular targeting property to the solid tumors in vivo. Pharm. Res. 18, 1042–1048.

Ishida, T., Ichihara, M., Wang, X., Kiwada, H., 2006. Spleen plays an important role in the induction of accelerated blood clearance of PEGylated liposomes. J. Control. Rel. 115, 243–250.

Joersbo, M., Brunstedt, J., 1990. Protein synthesis stimulated in sonicated sugar beet cells and protoplasts. Ultrasound Med. Biol. 16, 719–724.

Kawamura, K., Kadowaki, N., Suzuki, R., Udagawa, S., Kasaoka, S., Utoguchi, N., Kitawaki, T., Sugimoto, N., Okada, N., Maruyama, K., Uchiyama, T., 2006. Dendritic cells that endocytosed antigen-containing IgG-liposomes elicit effective antitumor immunity. J. Immunother. 29, 165–174.

Kim, H.J., Greenleaf, J.F., Kinnick, R.R., Bronk, J.T., Bolander, M.E., 1996. Ultrasound-mediated transfection of mammalian cells. Hum. Gene Ther. 7, 1339–1346.

Kinoshita, M., Hynynen, K., 2005a. Intracellular delivery of Bak BH3 peptide by microbubble-enhanced ultrasound. Pharm. Res. 22, 716–720.

Kinoshita, M., Hynynen, K., 2005b. A novel method for the intracellular delivery of siRNA using microbubble-enhanced focused ultrasound. Biochem. Biophys. Res. Commun. 335, 393–399.

Larina, I.V., Evers, B.M., Esenaliev, R.O., 2005. Optimal drug and gene delivery in cancer cells by ultrasound-induced cavitation. Anticancer Res. 25, 149–156.

Leong-Poi, H., Christiansen, J., Klibanov, A.L., Kaul, S., Lindner, J.R., 2003. Noninvasive assessment of angiogenesis by ultrasound and microbubbles targeted to alpha(v)-integrins. Circulation 107, 455–460.

Li, T., Tachibana, K., Kuroki, M., Kuroki, M., 2003. Gene transfer with echo-enhanced contrast agents: comparison between Albunex, Optison, and Levovist in mice—initial results. Radiology 229, 423–428.

Lindner, J.R., 2004. Microbubbles in medical imaging: current applications and future directions. Nat. Rev. Drug Discov. 3, 527–532.

Maruyama, K., Kennel, S.J., Huang, L., 1990. Lipid composition is important for highly efficient target binding and retention of immunoliposomes. Proc. Natl. Acad. Sci. U.S.A. 87, 5744–5748.

Maruyama, K., Ishida, O., Kasaoka, S., Takizawa, T., Utoguchi, N., Shinohara, A., Chiba, M., Kobayashi, H., Eriguchi, M., Yanagie, H., 2004. Intracellular targeting of sodium mercaptoundecahydrododecaborate (BSH) to solid tumors by transferrin-PEG liposomes, for boron neutron-capture therapy (BNCT). J. Control. Rel. 98, 195–207.

Miller, M.W., Miller, D.L., Brayman, A.A., 1996. A review of in vitro bioeffects of inertial ultrasonic cavitation from a mechanistic perspective. Ultrasound Med. Biol. 22, 1131–1154.

Miller, D.L., Pislaru, S.V., Greenleaf, J.E., 2002. Sonoporation: mechanical DNA delivery by ultrasonic cavitation. Somat. Cell Mol. Genet. 27, 115–134.

Mizuguchi, H., Nakagawa, T., Toyosawa, S., Nakanishi, M., Imazu, S., Nakanishi, T., Tsutsumi, Y., Nakagawa, S., Hayakawa, T., Ijuhin, N., Mayumi, T., 1998. Tumor necrosis factor alpha-mediated tumor regression by the in vivo transfer of genes into the artery that leads to tumors. Cancer Res. 58, 5725–5730.

Mosmann, T., 1983. Rapid colorimetric assay for cellular growth and survival: application to proliferation and cytotoxicity assays. J. Immunol. Methods 65, 55–63.

Shohet, R.V., Chen, S., Zhou, Y.T., Wang, Z., Meidell, R.S., Unger, R.H., Grayburn, P.A., 2000. Echocardiographic destruction of albumin microbubbles directs gene delivery to the myocardium. Circulation 101, 2554–2556.

Sonoda, S., Tachibana, K., Uchino, E., Okubo, A., Yamamoto, M., Sakoda, K., Hisatomi, T., Sonoda, K.H., Negishi, Y., Izumi, Y., Takao, S., Sakamoto, T., 2006. Gene transfer to corneal epithelium and keratocytes mediated by ultrasound with microbubbles. Invest. Ophthalmol. Vis. Sci. 47, 558–564.

Suzuki, R., Takizawa, T., Negishi, Y., Hagisawa, K., Tanaka, K., Sawamura, K., Utoguchi, N., Nishioka, T., Maruyama, K., 2007a. Gene delivery by combination of novel liposomal bubbles with perfluoropropane and ultrasound. J. Control. Rel. 117, 130–136.

Suzuki, R., Takizawa, T., Negishi, Y., Utoguchi, N., Maruyama, K., 2007b. Effective gene delivery with liposomal bubbles and ultrasound as novel nonviral system. J. Drug Target. 15, 531–537.

Suzuki, R., Takizawa, T., Negishi, Y., Utoguchi, N., Sawamura, K., Tanaka, K., Namai, E., Oda, Y., Matsumura, Y., Maruyama, K., in press. Tumor specific ultrasound enhanced gene transfer in vivo with novel liposomal bubbles. J. Control. Rel.

Tachibana, K., Tachibana, S., 1995. Albumin microbubble echo-contrast material as an enhancer for ultrasound accelerated thrombolysis. Circulation 92, 1148–1150.

Takahashi, M., Kido, K., Aoi, A., Furukawa, H., Ono, M., Kodama, T., 2007. Spinal gene transfer using ultrasound and microbubbles. J. Control. Rel. 117, 267–272.

Taniyama, Y., Tachibana, K., Hiraoka, K., Aoki, M., Yamamoto, S., Matsumoto, K., Nakamura, T., Ogihara, T., Kaneda, Y., Morishita, R., 2002a. Development of safe and efficient novel nonviral gene transfer using ultrasound: enhancement of transfection efficiency of naked plasmid DNA in skeletal muscle. Gene Ther. 9, 372–380.

Taniyama, Y., Tachibana, K., Hiraoka, K., Namba, T., Yamasaki, K., Hashiya, N., Aoki, M., Ogihara, T., Yasufumi, K., Morishita, R., 2002b. Local delivery of plasmid DNA into rat carotid artery using ultrasound. Circulation 105, 1233–1239.

Tata, D.B., Dunn, F., Tindall, D.J., 1997. Selective clinical ultrasound signals mediate differential gene transfer and expression in two human prostate cancer cell lines: LnCap and PC-3. Biochem. Biophys. Res. Commun. 234, 64–67.

Tsunoda, S., Mazda, O., Oda, Y., Iida, Y., Akabame, S., Kishida, T., Shin-Ya, M., Asada, H., Gojo, S., Imanishi, J., Matsubara, H., Yoshikawa, T., 2005. Sonoporation using microbubble BR14 promotes pDNA/siRNA transduction to murine heart. Biochem. Biophys. Res. Commun. 336, 118–127.

Wang, X., Ishida, T., Kiwada, H., 2007. Anti-PEG IgM elicited by injection of liposomes is involved in the enhanced blood clearance of a subsequent dose of PEGylated liposomes. J. Control. Rel. 119, 236–244.

Wei, W., Zheng-Zhong, B., Yong-Jie, W., Qing-Wu, Z., Ya-Lin, M., 2004. Bioeffects of low-frequency ultrasonic gene delivery and safety on cell membrane permeability control. J. Ultrasound Med. 23, 1569–1582.

Yamashita, T., Sonoda, S., Suzuki, R., Arimura, K., Tachibana, K., Maruyama, K., Sakamoto, T., in press. A novel bubble liposome and ultrasound-mediated gene transfer to ocular surface: RC:1 cells in vitro and conjunctiva in vivo. Exp. Eye Res.

Yanagie, H., Ogura, K., Takagi, K., Maruyama, K., Matsumoto, T., Sakurai, Y., Skvarc, J., Illic, R., Kuhne, G., Hisa, T., Yoshizaki, I., Kono, K., Furuya, Y., Sugiyama, H., Kobayashi, H., Ono, K., Nakagawa, K., Eriguchi, M., 2004. Accumulation of boron compounds to tumor with polyethylene-glycol binding liposome by using neutron capture autoradiography. Appl. Radiat. Isot. 61, 639–646.

Yanagie, H., Maruyama, K., Takizawa, T., Ishida, O., Ogura, K., Matsumoto, T., Sakurai, Y., Kobayashi, T., Shinohara, A., Rant, J., Skvarc, J., Ilic, R., Kuhne, G., Chiba, M., Furuya, Y., Sugiyama, H., Hisa, T., Ono, K., Kobayashi, H., Eriguchi, M., 2006. Application of boron-entrapped stealth liposomes to inhibition of growth of tumour cells in the in vivo boron neutron-capture therapy model. Biomed. Pharmacother. 60, 43–50.

J Med Ultrasonics (2008) 35:5–10
DOI 10.1007/s10396-007-0163-x

ORIGINAL ARTICLE

Taira ZENITANI · Ryo SUZUKI · Kazuo MARUYAMA
Hiroshi FURUHATA

Accelerating effects of ultrasonic thrombolysis with bubble liposomes

Received: May 23, 2007 / Accepted: September 28, 2007

Abstract
Purpose. The accelerating effect on thrombolysis by combined use of 500-kHz low-frequency ultrasound (US), recombinant tissue plasminogen activator (rt-PA), and bubble liposomes (BLs) was verified in vitro.
Methods. A fibrin clot was formed by adding thrombin to bovine plasma. It was enclosed in a pressurized container, the pressure and temperature of which were maintained at 150 mmHg and 37°C, respectively. Ultrasonic conditions were set at a continuous wave, a frequency of 500 kHz, an intensity of 0.7 W/cm^2, and a sonication time of 60 s. We derived the rate of reduction in clot weight from the decreased clot weight and the weight before sonication. We compared the rate of reduction in groups combining physiological saline, rt-PA, BLs, and US.
Results. Only the rt-PA+US+BL group showed a significantly accelerated thrombolytic effect compared with any other group or with any combination of two factors in the 60-s period ($0.001 < P < 0.027$).
Conclusion. BLs have great potential to accelerate the thrombolytic effect of rt-PA with low-frequency, 500-kHz, continuous-wave ultrasound.

Keywords ultrasound · thrombolysis · bubble · liposome

Introduction

As clot recanalization therapy for acute myocardial infarct and more recently for acute cerebral infarct, a thrombolytic agent with a high affinity for clots, i.e., recombinant tissue plasminogen activator (rt-PA), is intravenously administered.[1,2] For all acute ischemic conditions, the sooner blood flow recanalization is achieved, the better the outcome. Hence, as a measure to enhance the thrombolytic effect of rt-PA, the combined use of ultrasound (US) was developed with limited application in clinical practice. It has been shown that monitoring with diagnostic transcranial Doppler (TCD) ultrasound (US) at 2 MHz with rt-PA treatment increases the recanalization rate 2 h after the procedure in most acute ischemic stroke cases in which urgent ischemic recanalization is indicated.[3] On the other hand, although still at the in vitro/in vivo experimental stage, a study showed that for ultrasonography in the range of some tens of kilohertz, i.e., lower than the diagnostic megahertz range, 1 h of radiation-accelerated thrombolysis yielded higher thrombolytic rates than the diagnostic US range did.[4] However, the outcome was neurologically evaluated at 3 months and improvement was still seen in only 20%–30% of cases.

As a technology to further improve the thrombolysis-enhancing effects of this US treatment, the efficacy of microbubbles (MBs), a US contrast medium, has also been demonstrated clinically. A study showed that with rt-PA administration, if additional contrast medium was administered to acute cerebral infarct patients during TCD monitoring, the complete recanalization rate 2 h after the procedure was 40.8% for those co-administered rt-PA and TCD, whereas adding MBs increased the rate significantly to 54.5%.[5]

For the latest treatment currently given to patients with ischemic disease, i.e., a combination of thrombolytic agents, US, and MBs, the recanalization time is not yet clinically satisfactory. In dealing with these problems, in terms of the US conditions and MBs, the following technical challenges remain. As to the US conditions, instead of the diagnostic wavelength range, utilization of the range between some tens and some hundreds of kilohertz, for which efficacy has not been well documented in either in vitro or in vivo studies, may be considered.[6–8] Improvement in thrombolytic recanalization rates and shortening of the recanalization time are anticipated in the clinical setting with low-frequency, low-intensity US. Moreover, enhanced efficacy by employing additional MBs may be associated with clot

T. Zenitani (✉) · H. Furuhata
Medical Engineering Laboratory, Research Center for Medical Science, Jikei University School of Medicine, 3-25-8 Nishishinbashi, Minato-ku, Tokyo 105-8461, Japan
Tel. +81-3-3433-1111; Fax +81-3-3459-6005
e-mail: taira_z@jikei.ac.jp

R. Suzuki · K. Maruyama
Department of Biopharmaceutics, School of Pharmaceutical Sciences, Teikyo University, Tsukui, Japan

surface invasion by bubble breakthrough. Currently, a variety of imaging media are commercially available, but their bubbles are several micrometers in diameter, and no studies have examined the efficacy of applying bubbles with a diameter of several hundreds of nanometers, which are highly likely to penetrate clots.

This study, in an effort to achieve shorter thrombolysis times, employed a 500-kHz continuous wave (CW) US, which one of the present authors had been examining for US conditions,[7] because this is the only condition for which the efficacy and safety of the TCD method have been shown in animal experiments. We employed perfluoropropane (PFP)-enclosed bubbles, i.e., novel bubble liposomes (BLs) based on the liposomes prepared by Suzuki et al.[9,10] Because these BLs contain bubbles with a diameter of several hundreds of nanometers, they may pass through 5-μm fibrin nets, thereby invading clots more effectively. For evaluation of the thrombolytic time-shortening effect in particular, we conducted an in vitro study of rt-PA, US, and BLs to assess clot weight loss rates at 1 min after application. Since the effects of a conventional combination of rt-PA and US are reportedly expressed approximately 5 min after application,[11] we compared the efficacy in as little as one-fifth of this time to clarify the efficacy of a shorter time period.

Subjects and methods

Preparation of BLs

We prepared BLs in accordance with the method proposed by Suzuki et al.[9,10] First, 2 ml of liposome solution (NOF, Japan) (lipid content 1 mg/ml) and 5 ml of PFP (Takachiho, Japan) were placed in a 5-ml vial that was then tightly closed. Another 7.5 ml of PFP was added and then irradiated with 42-kHz US in an ultrasonic cleaner (2510J-DTH, Branson Ultrasonics/Emerson Japan, Japan) to prepare the BLs. The almost clear liposome solution became cloudy as a result of this procedure. The particle size distributions of these BLs and liposome solution were measured using a dynamic light-scattering particle size distribution meter (Zetasizer, Sysmex). At the same time, we observed BLs using a light microscope (Eclipse 80i, NIKON) and a digital finescope (VC7700, Omron).

Measurement of BL elimination rate and determination of acoustic intensity

Figure 1a depicts BLs before US radiation and Fig. 1b shows BLs after US radiation. Clear cellophane was spread on the bottom of each cylindrical acrylic tube with an inside diameter of 1 cm, and 1 ml of BL solution was infused. The US used was a CW generated by a circular Lead Titanate Ziroonate transducer (Φ 10 mm) (Honda Electronics, Japan) at 500 kHz and an acoustic intensity of 0.7 W/cm^2 spatial peak temporal average (SPTA). The exposure time was 60 s (amplifier, high-speed power amplifier 4055, NF, Japan; signal generator, Wave factory 1941, NF). From the bottom of this cylinder, US radiation was used to measure the mean luminance of BLs in the central part of the container (Fig. 1, central circle) before and after exposure to US radiation. The postradiation value was subtracted from the preradiation value and then divided by the preradiation value to determine the BL elimination rate (this technique is hereinafter referred to as the scattering light simplified measurement method). For different levels of the acoustic intensity, each cylinder was measured five times to determine the mean value. The best acoustic intensity was thus determined to be 0.7 W/cm^2, based on the acoustic intensity versus BL elimination curve, and this level was employed in the study.

Verification of the thrombolysis effect

In this study, we used a fibrin clot prepared by treating bovine plasma (Sigma-Aldrich, Japan) with 20 μl of thrombin (100 IU/ml) (Sigma-Aldrich). In order to minimize the contact area, the clot was encapsulated in a pressurized container using a pincette with a thin diffracted tip (Suncraft, Japan) to prevent the fibrin clot from breaking. Then, while measuring the pressure in the container using a manometer (DG-100-102GP, Copal Electronics, Japan), it was gradually pressurized with a 5-ml syringe to 150 mmHg

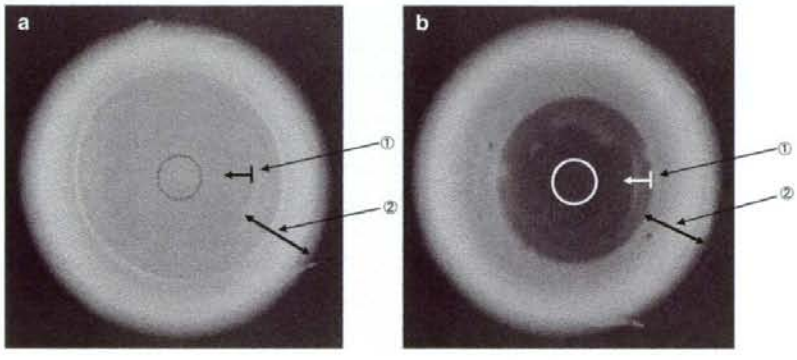

Fig. 1a,b. Changes in the luminosity of a bubble liposome (BL) solution. The average luminosity in the *circle* was measured: **a** BLs before sonication and **b** BLs after sonication [continuous wave (CW), 500 kHz, 0.7 W/cm^2, 60 s]. *1*, BLs; *2*, acrylic tube

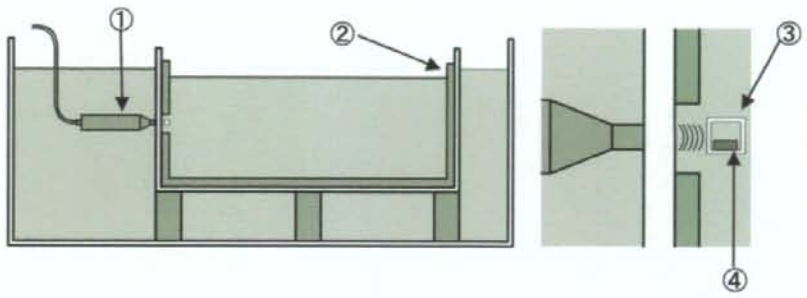

Fig. 2. Experimental system for sonication: *1*, 500-kHz transducer; *2*, sound-absorbing foam; *3*, container; *4*, fibrin clot

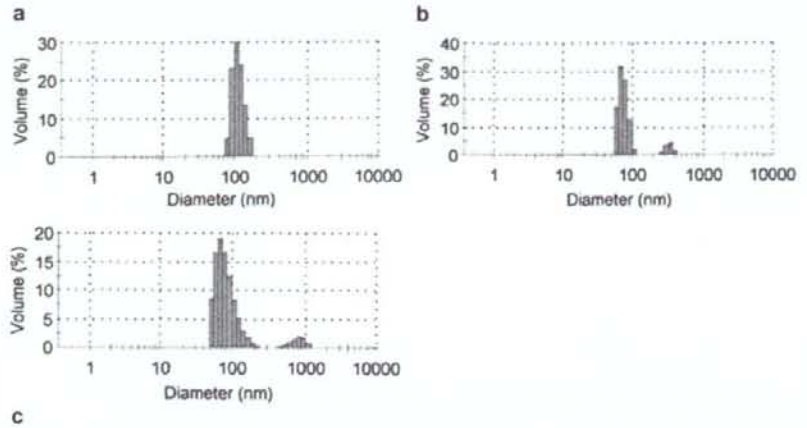

Fig. 3. Size distribution by dynamic light scattering. **a** Liposomes measured within 2 min of shaking are mostly 120 nm in diameter. **b** BLs measured within 2 min of shaking: 50–100 nm and 200–400 nm. **c** BLs measured from 2 to 4 min after shaking: 50–200 nm and 1 μm or more

and 37°C. Then, US radiation was applied using the setup shown in Fig. 2. The thrombolytic effect was evaluated by the fibrin clot weight loss rates. Because the fibrin clot should be weighed after the elimination of water content around the clot, the fibrin clot was placed on a 50-μm mesh (PET51-HC, Tanaka Sanjiro, Japan), and the water filtering through the mesh was absorbed with absorbent paper (Kimwipe Wiper S-200, Nippon Paper Crecia, Japan) for measurement with an analytical balance (AB104-S, Mettler Toledo, Switzerland) (minimum indication: 0.1 mg). Without directly touching the clot so as to avoid losing water contained in the fibrin clot, we simply replaced the absorbent paper placed under the mesh. The weight loss rates were determined as (pre-encapsulation weight – post-US radiation weight)/pre-encapsulation weight. The time from fibrin clot encapsulation to measurement of post-US radiation weight was set at 3 min. The US conditions were set as determined above, i.e., CW, 500 kHz, 0.7 W/cm^2 (SPTA), and 60 s. The acoustic intensity was measured in a nonpressurized container using a needle-type hydrophone (HNC-0400, ONDA, CA, USA). We used the following four types of solutions: physiological saline (control group), physiological saline solution prepared with BLs at 0.5 mg/ml (BL group), physiological saline solution prepared with rt-PA (monteplase) at 1000 IU/ml (rt-PA group), and physiological saline solution prepared with rt-PA at 1000 IU/ml and BLs at 0.5 mg/ml (rt-PA + BL group).

Evaluation method

We compared groups using the *t* test to confirm that there were no differences in pre-US radiation fibrin clot weight between any of the groups. Then, for the control, rt-PA, BL, and rt-PA + BL groups with and without US radiation, i.e., a total of eight groups (control, rt-PA, BL, rt-PA + BL, US, rt-PA + US, BL + US, and rt-PA + BL + US groups), ten clots per group were statistically compared using the *t* test.

Results

BL particle size distribution

The particle size distribution of liposomes and BLs determined by the dynamic light scattering method are presented in Figs. 3a–c. Fig. 3a presents the particle size distribution of the liposomes, showing a central diameter of approximately 120 nm and a distribution range of 70–200 nm. Figures 3b and 3c present the analytical results for the BL particle distribution at 0–2 min and 2–4 min after shaking by hand, respectively. The distributions in the two groups were between 50 and 100 nm and between 200 and 400 nm at 0–2 min. At 2–4 min, the distribution range widened and was divided into one group at 50–200 nm and another at more

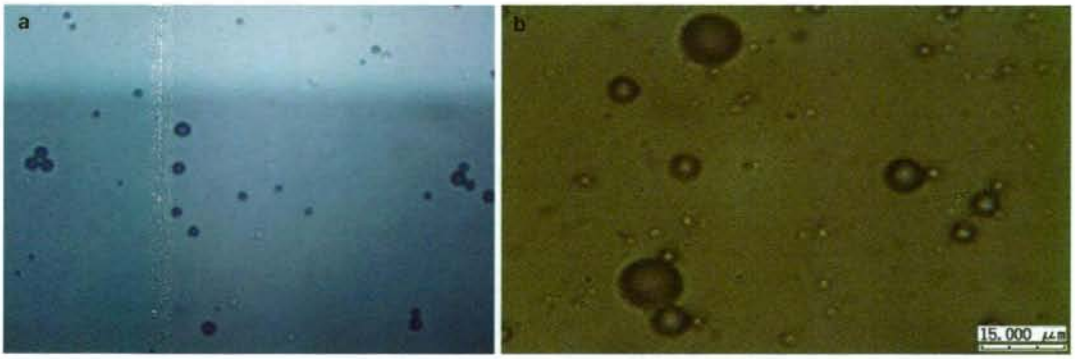

Fig. 4a,b. Photomicrographs of BLs. **a** Light microscopic view (×400) and **b** digital finescope view (×7000)

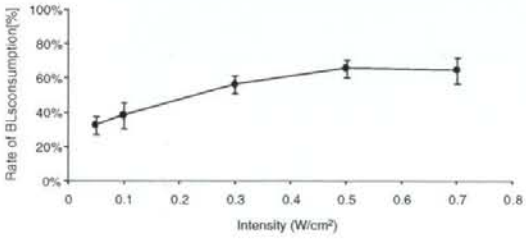

Fig. 5. Relation between ultrasound (US) intensity (CW, 500 kHz, 60 s) and rate of BL consumption: 62% at the maximum intensity 0.5 W/cm^2 ($n = 3$)

than 1 µm. This may be because the BL concentration fluctuates within the observation range of 100 µm, and the distribution changes with time. This phenomenon is shown in Figs. 3b and 3c.

Observations made with a light microscope and a digital finescope are presented in Figs. 4a and 4b, respectively. The prepared BLs were observed to vary in size and to change over time. There were some micro-orders not measurable with the dynamic light scattering method.

Occurrence of microcavitation

Figure 5 shows the BL elimination rate for various levels of acoustic intensity using the scattering light simplified measurement method. The higher the acoustic intensity, the higher the BL elimination rate, and when the intensity exceeded approximately 0.5 W/cm^2, the elimination rate showed a roughly constant value. From these results, the acoustic intensity for the experiments was set at 0.7 W/cm^2. This acoustic intensity was determined under nonpressurized conditions.

Weight reduction rate

Figure 6a shows a prepared fibrin clot. The photograph was taken with the fibrin clot placed on a 50-µm mesh. The elastic, yellowish-white, cylindrical fibrin clots were encapsulated in a pressurized container and radiated with US. Figure 6b shows the fibrin clot after US radiation; the size was clearly reduced.

Figure 7 shows that there were no differences in fibrin clot weight among the groups before US radiation. Figure 8 shows the weight reduction rates for fibrin clots in each solution with or without US radiation. Comparisons among the control, BL, and BL + US groups revealed the mean clot weight reduction rate and variances to be 24.2 ± 3.6%, 24.9 ± 4.8%, and 25.8 ± 3.2%, respectively, and when BLs were administrated alone or with US radiation (500 kHz), no enhancement of thrombolysis was observed (P>0.05). A comparison between the control and rt-PA groups revealed weight reduction rates of 24.2 ± 3.6% and 24.2 ± 2.8%, respectively, with no significant difference (P = 0.30), and exposure to US did not enhance the thrombolytic effect of rt-PA. There were no differences in individual single-drug effects or weights in relation to the two active elements.

However, compared with the other seven groups, the rt-PA + BL + US group exhibited a significantly increased weight reduction (29.2 ± 3.0%, 0.001 < P < 0.027). There were no significant differences among the other two groups except for the rt-PA + BL + US group (0.25 < P < 0.99). Based on these results, the significant enhancement of thrombolytic rate observed for the rt-PA + BL + US group was the result of the three overlapping effects of the individual treatments.

Discussion

In this study, a combination of rt-PA, BLs, and US increased the thrombolytic rate of bovine fibrin clots after 1 min. To date, studies have reported the enhancement of thrombolysis with MBs, but herein it was shown that BLs may accelerate thrombolysis when applied with rt-PA and US.

Siegel et al. reported that a combination of perfluorocarbon-exposed sonicated dextrose albumin (PESDA) and percutaneous US radiation (37 kHz, 160 W max., 60 min) resulted in 100% recanalization in a rabbit clot infarction

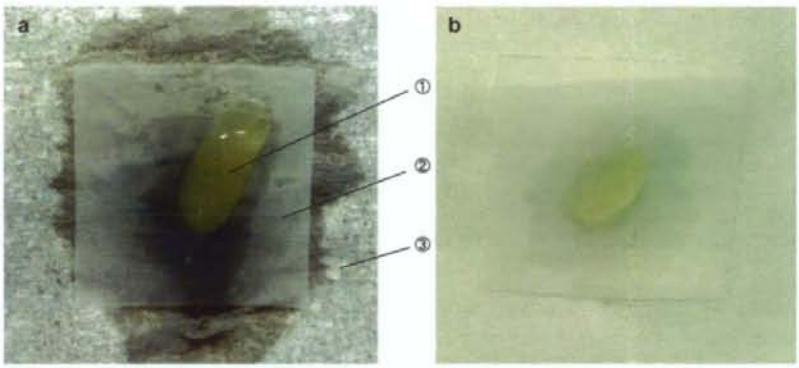

Fig. 6. A fibrin clot **a** before sonication (*1*, fibrin clot; *2*, 50-μm mesh; *3*, absorption paper) and **b** after sonication

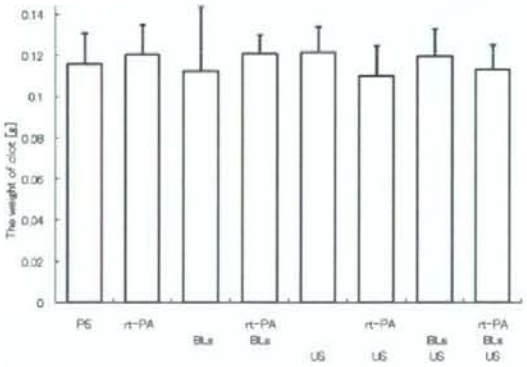

Fig. 7. Weight of clots before sonication. There were no differences in the clot weights before sonication among the groups. Data are expressed as mean ± SD (n = 10). *PS*, physiological saline; *rt-PA*, recombinant tissue plasminogen activator

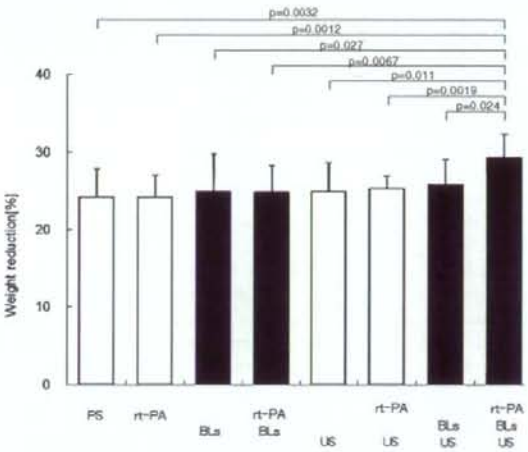

Fig. 8. Comparison of the rates of decrease in fibrin clot weight under various treatments: rt-PA (monteplase 1000 IU/ml), BLs (lipid 0.5 mg/ml), US (CW, 500 kHz, 60 s). Compared with any other group or with any combination of two factors, the clot weight reduction was significantly larger for the rt-PA+BL+US group ($P < 0.05$). Data are expressed as mean ± SD (n = 10)

model.[12] They employed US at approximately one-tenth of the frequency used in our experiments, and the mechanical index (MI) was about 3.3 times greater (MI is actually defined by the pulse wave, and so MI is not directly applicable to CW, or a burst wave, but there is no other appropriate index, and MI was thus applied). Although our BLs had a lower MI than those of Siegel et al, adding rt-PA enhanced the thrombolytic rate obtained at 1 min.

Mizushige et al. also showed that a combination of rt-PA and US radiation (CW, 10 MHz, 1.02 W/cm^2, 10 min) in addition to MBs [dodecafluoropentane (DDFP)] yielded a clot weight reduction rate of 49% in an in vitro study of human white thrombi.[13] Compared with their experimental conditions, our frequency was 1/20 and the exposure time was 1/10, and because of clot variations we cannot compare our results with theirs directly, but we did compare the weight reduction rates: 29% for the rt-PA + BL + US group versus 49%. The superimposed effects of the three elements, rt-PA, BLs, and US, may increase thrombolytic rates even at 10 min after administration; such temporal changes will be examined further.

Spengos et al. conducted a study evaluating temporal increases in thrombolytic rates using a flow model.[11] The starting point of increases in recanalization flow was 15 min for use of rt-PA alone, but this was shortened to 5 min with the combination of rt-PA and 1-MHz US exposure, and increased thrombolytic rates were observed when rt-PA was enhanced by US. However, even though they used the same bovine fibrin clot that we did, no enhanced recanalization flow was observed at 1 min after application. We did not evaluate such temporal changes but we did show that within 1 min, while no thrombolytic effect was observed in their study, the superimposed effects of the three elements, including BLs, enhanced the thrombolytic rates in our model.

The achievement of enhanced thrombolytic rates in as short a time as 1 min may be largely attributable to the

newly included BLs. For clots, single use of rt-PA or 500-kHz low-frequency US or a combination of these two modalities does not enhance thrombolysis after 1 min. However, adding BLs to these two elements enhanced thrombolytic rates, i.e., shortened the thrombolysis time.

The enhanced thrombolytic rates achieved by BLs may be due to the presence of nanosized particles, a characteristic distinguishing BLs from other MBs. The particle size distribution of BLs was measured using the dynamic light scattering method, which was limited to a detection area 100 μm in diameter and was designed to be used for uniformly dissolved substances. The particle size distribution of BLs measured with the dynamic light scattering method changed with time, suggesting that the delicate condition within the small detection range may fluctuate on an hourly basis. It was suggested that BLs might contain very small bubbles of approximately 120 nm in diameter and larger bubbles with diameters of 1–2 μm. However, cumulative formation of microsized air bubbles via aggregation of very small air bubbles of about 100 μm in diameter should also perhaps be considered. We prepared BLs using the same technique as that of Suzuki et al., though their BLs were approximately 3 μm in size, whereas ours contained massive bubbles. We will conduct further studies to ascertain why this difference in bubble size distribution occurred. In addition, we will also compare our bubbles with other bubbles.

Because the pore space of the fibrin net in clots is approximately 5 μm,[14] BLs containing nanosized particles in addition to microsized particles may pass through these pores. However, as clarified by the experiments, even though BLs alone permeated the fibrin net, no enhancement of the thrombolytic rate was observed.

Francis et al. proposed that 1-MHz, 4-W/cm^2 US radiation reversibly extended the fibrin structure, facilitating rt-PA penetration.[15] However, the present experiment employed US conditions different from those in their report, and because of the one-half frequency and one-sixth acoustic intensity used herein, only slight fibrin structure extension may have occurred.

Tachibana, using electron micrography, reported how microjets generated on the elimination of MBs were hitting cell surfaces.[16] Even in the absence of an extended fibrin structure due to this physical phenomenon, microjets generated around the fibrin clot by cavitation may have enhanced infiltration of BLs and rt-PA into the fibrin clot.

As a result, the superimposed effects of the three elements (BLs containing submicrosized particles, US-generated microjets and microvibration, and rt-PA) appear to have yielded enhanced clot thrombolytic rates.

The present study used thrombin–fibrin clots. In clinical practice, we see atherothrombosis and platelet thrombus in addition to thrombin clots, and whether results similar to those described here would be obtained with these clots is unknown. The efficacy against these types of clots needs to be examined further.

Conclusion

We confirmed that bubble liposomes with rt-PA and low-frequency US increased thrombolytic rates even in a very short time, i.e., in as little as 1 min.

References

1. The GUSTO investigators. An international randomized trial comparing four thrombolytic ratagies for actice myocardial infarction. The GUSTO investigators. N Engl J Med 1993;329(10):673–82.
2. The National Institute of Neurological Disorders and Stroke rt-PA Stroke Study Group. Tissue plasminogen activator for acute ischemic stroke. N Engl J Med 1995;333:1581–7.
3. Alexandrov AV, Molina CA, Grotta Z, et al. Ultrasound-enhanced systemic thrombolysis for acute ischemic stroke. N Engl J Med 2004;351:2170–8.
4. Suchkova V, Siddiqi FN, Carstensen EL, et al. Enhancement of fibrinolysis with 40-kHz ultrasound. Circulation 1998;98:1030–5.
5. Molina CA, Ribo M, Rubiera M, et al. Microbubble administration accelerates clot lysis during continuous 2-MHz ultrasound monitoring in stroke patients treated with intravenous tissue plasminogen activator. Stroke 2006;37(2):425–9.
6. Behrens S, Daffertshofer M, Spiegel D, et al. Low-frequency, low-intensity ultrasound accelerates thrombolysis through the skull. Ultrasound Med Biol 1999;25(2):269–73.
7. Ishibashi T, Akiyama M, Onoue H, et al. Can transcranial ultrasonication increase recanalization flow with tissue plasminogen activator? Stroke 2002;33:1399–1404.
8. Tachibana K, Tachibana S. Albumin microbubble echo-contrast material as an enhancer for ultrasound-accelerated thrombolysis. Circulation 1995;92(5):1148–50.
9. Suzuki R, Takizawa T, Negishi Y, et al. Gene delivery by combination of novel liposomal bubbles with perfluoropropane and ultrasound. J Controlled Release 2007;117(1):130–6.
10. Suzuki R, Takizawa T, Negishi Y, et al. Tumor-specific ultrasound-enhanced gene transfer in vivo with novel liposomal bubbles. J Controlled Release 2008;125(2):137–44.
11. Spengos K, Behrens S, Daffertshofer M, et al. Acceleration of thrombolysis with ultrasound through the cranium in a flow model. Ultrasound Med Biol 2000;26(5):889–95.
12. Siegel RJ, Atar S, Fishbein MC, et al. Noninvasive transcutaneous low-frequency ultrasound enhances thrombolysis in peripheral and coronary arteries. Echocardiography 2001;18(3):247–57.
13. Mizushige K, Kondo I, et al. Enhancement of ultrasound-accelerated thrombolysis by echo contrast agents: dependence on microbubble structure. Ultrasound Med Biol 1999;25(9):1431–7.
14. Carr ME Jr, Hardin CL. Fibrin has larger pores when formed in the presence of erythrocytes. Am J Physiol 1987;253(5 Pt 2): H1069–73.
15. Francis CW, Blinc A, Lee S, et al. Ultrasound accelerates transport of recombinant tissue plasminogen activator into clots. Ultrasound Med Biol 1995;21(3):419–24.
16. Tachibana K. Application of microbubbles for therapy. Med Biol Eng 2005;43(2):211–5.

Nucleic Acids Research Advance Access published February 22, 2009

Nucleic Acids Research, 2009, 1–15
doi:10.1093/nar/gkp066

Massive transcriptional start site analysis of human genes in hypoxia cells

Katsuya Tsuchihara[1], Yutaka Suzuki[2,*], Hiroyuki Wakaguri[2], Takuma Irie[2], Kousuke Tanimoto[2], Shin-ichi Hashimoto[3], Kouji Matsushima[3], Junko Mizushima-Sugano[2,4], Riu Yamashita[5], Kenta Nakai[5], David Bentley[6], Hiroyasu Esumi[1] and Sumio Sugano[2]

[1]Cancer Physiology Project, Research Center for Innovative Oncology, National Cancer Center Hospital East: 6-5-1 Kashiwanoha, Kashiwa, Chiba 277-8577, [2]Graduate School of Frontier Sciences, the University of Tokyo: 5-1-5 Kashiwanoha, Kashiwa, Chiba 277-8562, [3]Graduate School of Medicine, the University of Tokyo: 7-3-1 Hongo, Bunkyokyu, Tokyo 113-0033, [4]Laboratory of Molecular Virology, Kitasato Institute for Life Sciences, Kitasato University: 5-9-1 Shirokane, Minatoku, Tokyo 108-8641, [5]Institute of Medical Science, the University of Tokyo: 4-6-1 Shirokenedai, Minatoku, Tokyo 108-8639, Japan and [6]Illumina, Inc: 25861 Industrial Boulevard Hayward, CA 94545, USA

Received October 3, 2008; Revised January 20, 2009; Accepted January 22, 2009

ABSTRACT

Combining our full-length cDNA method and the massively parallel sequencing technology, we developed a simple method to collect precise positional information of transcriptional start sites (TSSs) together with digital information of the gene-expression levels in a high throughput manner. We applied this method to observe gene-expression changes in a colon cancer cell line cultured in normoxic and hypoxic conditions. We generated more than 100 million 36-base TSS-tag sequences and revealed comprehensive features of hypoxia responsive alterations in the transcriptional landscape of the human genome. The features include presence of inducible 'hot regions' in 54 genomic regions, 220 novel hypoxia inducible promoters that may drive non-protein-coding transcripts, 191 hypoxia responsive alternative promoters and detailed views of 120 novel as well as known hypoxia responsive genes. We further analyzed hypoxic response of different cells using additional 60 million TSS-tags and found that the degree of the gene-expression changes were different among cell lines, possibly reflecting cellular robustness against hypoxia. The novel dynamic figure of the human gene transcriptome will deepen our understanding of the transcriptional program of the human genome as well as bringing new insights into the biology of cancer cells in hypoxia.

INTRODUCTION

Aberrantly growing cancer cells in solid tumors frequently encounter a shortage of blood flow, which leads to insufficient oxygen supply. Tumor cells adapt themselves to such hypoxic microenvironment by shifting their ATP production metabolism from oxidative phosphorylation to anaerobic glycolysis, and by enhancing glucose intake. Tumor cells also induce angiogenesis to acquire additional blood supplies. Such adaptations are supposed to be essential in survival as well as malignant transformation of tumor cells *in vivo* (1,2). During this series of events, transcriptional regulation plays a pivotal role. It has been well documented that hypoxia inhibits proteasomal degradation of α subunits of hypoxia inducible factors (HIF1α and HIF2α). Stabilized subunits translocate from the cytoplasm into the nucleus and form a heterodimer complex with HIF1β. HIF complexes transactivate various downstream genes, such as the genes encoding glycolytic enzymes, glucose transporters, the enzymes eradicating organic acids and VEGF which induces angiogenesis. However, the specific function of each isoform of the subunits remains unclear. Meanwhile, 'HIF-independent' regulation of hypoxia-inducible genes has also been documented (3,4). Thus, the current view of hypoxic versatility in transcriptome programs in cancer cells is still far from comprehensive. A bird's eye view on what range of genes are induced in what manner still remains mostly elusive. Although some genome-wide expression profiles using microarrays have been reported, they represent mere collective information of the fold inductions of the individual genes (5–9). In this regards, we believed that information

*To whom correspondence should be addressed. Tel/Fax: +81 4 7136 3607; Email: ysuzuki@k.u-tokyo.ac.jp

about exact positions of transcriptional start sites (TSSs) and absolute levels of the transcriptions starting from them would lead to more comprehensive understandings.

Several methods based on cDNA analysis have been developed for large-scale identification of TSSs (10–13). We have also developed a method to selectively replace the cap structure of the mRNA with a synthetic oligo, which we named the oligo-capping method (11). By sequencing 1.8 million cDNAs isolated from oligo-cap cDNA libraries from various kinds of human cells and tissues (14), we have collected the positional information of the TSS and analyzed putative proximal promoter regions (15,16). We, as well as another research group in RIKEN, have further improved the efficacy of this approach by combining the cap-selection method with the SAGE method (17,18). In these methods, 5′-ends of full-length cDNAs were concatenated, so that 10–15 20-base long 5′-end tag sequences could be identified by single-pass sequencing. By intensive analysis of CAGE-tag libraries in humans and mice, the FANTOM consortium reported a first glimpse of the transcription landscape of mammalian genomes (19,20). However, such an overview of the TSSs has been obtained from collective analysis of various cell types and tissues, for each of which the data coverage still remains scarce. Therefore, it does not represent the actual transcriptional landscape in any given cell type. Besides, it has been suggested recently that mammalian genes seem to utilize multiple alternative promoters very frequently, which enable a single locus to encode functionally distinct proteins, thereby serving as a molecular basis for realizing multifaceted use of a limited number of human genes (21,22). Nonetheless, the depth of the analysis has not reached the level of these alternative promoters, whose expression levels are often low and limited to particular cell types or cellular environments.

Recently developed massively parallel sequencing technologies have provided a potential mean to further improve the throughput of TSS identification. For example, Illumina GA sequencer (23) can sequence 10–30 million sequences per run. Although the read length which this sequencer can generate is short (currently up to 36 bases), it is sufficient to uniquely determine the precise positions of TSS. By combining oligo-capping method with the Illumina GA technology, we developed a simple method to collect information of the TSS together with the digital data of the expression levels of the transcripts. Here we show this approach enabled us to see the genome wide transcriptional landscape in response to hypoxia in a human colorectal cancer cell line.

MATERIALS AND METHODS

Cell culture and RNA interference

Human cell line, DLD-1 cells, was purchased from American Type Culture Collection (ATCC number: CCL-221). Cells were maintained in Dulbecco's modified Eagle's medium (DMEM) (Invitrogen) supplemented with 10% fetal calf serum, 4.5 g/l glucose, and antibiotics. RNA interference was accomplished by transfecting DLD-1 cells with the specific siRNA. HIF1A and EPAS1 (HIF2A)-targeting siRNA pool and non-silencing siRNA pool were purchased from Dharmacon. Short oligo-RNAs were transfected using Dharmafect 1 transfection reagent (Dharmacon) as recommended by the manufacturer. For constructing other TSS-libraries, HEK293, MCF7 and TIG3 cells (ATCC number: CRL-1573, ATCC number: HTB-22 and Japan Cell Resource Bank number: JCRB0506, respectively) were cultured in standard conditions and were subjected to the hypoxic shocks in a similar manner.

Oligo-capping and massively parallel sequencing by Illumina GA Sequencer

Six million DLD-1 cells were seeded 24 h before transfection. The cells transfected with HIF-targeting and control siRNA were cultured in 21% O_2 and 5% CO_2 at 37°C for 24 h followed by incubation in 21% O_2 or 1% O_2 and 5% CO_2 for 24 h. Cells were harvested and RNA was extracted using RNeasy (Qiagen). Two hundred microgram of the obtained total RNA was subjected to oligo-capping with some modifications from the original protocol; namely after the successive treatment of the RNA with 2.5 U BAP (TaKaRa) at 37°C for 1 h and 40 U TAP (Ambion) at 37°C for 1 h, the BAP-TAP-treated RNAs were ligated with 1.2 μg of RNA oligo (5′-AAUGAUACGGCGACCACCGAGAUCUACACU CUUUCCCUACACGACGCUCUUCCGAUCUGG-3′) using 250 U T4 RNA ligase (TaKaRa) at 20°C for 3 h. After the DNase I treatment (TaKaRa), polyA-containing RNA was selected using oligo-dT powder (Collaborative). First strand cDNA was synthesized from 10 pmol of random hexamer primer (5′-CAAGCAGAAGACGGCA TACGANNNNNNC-3′) using Super Script II (Invitrogen) by incubating at 12°C for 1 h and at 42°C overnight. Template RNA was degraded by alkarine treatment. For PCR, one-fifth of the first strand cDNAs were used as the PCR template. Gene Amp PCR kits (PerkinElmer) were used with the PCR primers 5′-AAT GATACGGCGACCACCGAG-3′ and 5′-CAAGCAGA AGACGGCATACGA-3′ under the following reaction conditions: 15 cycles of 94°C for 1 min, 56°C for 1 min and 72°C for 2 min. The PCR fragments were size fractionated by 12% polyacrylamide gel electrophoresis and the fraction of 150–250 bp was recovered. The quality and quantity of the obtained single-stranded first strand cDNAs were assessed, again, using BioAnalyzer (Agilent).

One nanogram of the size fractionated cDNA was used for the sequencing reactions with the Illumina GA. 15 000–20 000 clusters were generated per 'tile' and 36 cycles of the sequencing reactions were performed according to the manufacturer's instructions.

Data processing

The obtained sequences were mapped onto human genomic sequences (hg18 as of UCSC Genome Browser; http://genome.ucsc.edu/) using the sequence alignment program Eland. Unmapped or redundantly mapped sequences were removed from the dataset. For uniquely mapped sequences, relative positions to RefSeq genes were calculated based on the respective genomic coordinates.

Genomic coordinates of exons and other information of the RefSeq transcripts are as described in hg18 as of UCSC Genome Browser. GO (as of June 14th, 2007) and KEGG (Release 42) terms were associated with RefSeq genes by using loc2go (as of June 14th, 2007) using NCBI Entrez Gene database (http://www.ncbi.nlm.nih.gov/sites/entrez?db=gene). For each RefSeq gene, a RefSeq region was defined as the region from 50 kb upstream of the most upstream 5′-end exon to the most downstream 3′-end exon. TSS-tags were further clustered into 500-bp bins to generate TSS clusters (TSCs). Details and rationalization of the procedure is described in the ref. (15). For the expression analysis at the gene levels, TSS-tag counts of TSCs belonging to the corresponding RefSeq regions were totalled. For the expression analyses at the alternative promoter level, intergenic and antisense transcripts, the TSS-tags belonging to the corresponding TSCs were counted. In either case, TSS-tag counts were divided by the total number of uniquely and perfectly (with no mismatch) mapped TSS-tag to calculate TSS-tag ppm (parts per million). For the analysis of intergenic TSCs, overlap between the TSCs and miRNA and snoRNA, from miRBase (http://microrna.sanger.ac.uk/sequences/index.shtml) and snoRNABase (http://www-snorna.biotoul.fr/index.php), respectively, were examined.

Validation analysis

Real-time RT–PCRs were performed using 7900HT (ABI) following the standard protocol. PCR primer sequences are shown in the Supplementary Table 10. For the RT–PCR, 1 ng of the first strand cDNAs, which were synthesized by random hexamer primer, was used. In the case of plasmids, 1 pg of the DNA, quantified by O.D., was used, instead. The primer sets were first tested by amplifying the plasmid DNA and the primer sets giving less that 35 Ct cycles were used. The absolute copy number of each transcript in the cDNA population was calculated based on the Ct value of the corresponding plasmid (as 2^{deltaCt}). Based on the quantitative data, correlation with the digital expressions (TSS-tag counts) was calculated by linear regression. Validation analysis of the fold induction was similarly performed without the plasmid control. RNA independently isolated from the DLD-1 cells cultured in similar hypoxia (1% O_2) and normoxia (21% O_2) conditions were used. The samples were normalized according to the total amount of the first strand cDNAs and were subjected to the real-time RT–PCR.

For the individual oligo-cap RACE, similarly isolated total RNAs were oligo-capped with the RNA oligo (5′-AGCAUCGAGUCGGCCUUGUUGGCCUACUGG-3′) by the standard protocol. After the DNaseI treatment, the first strand cDNA was synthesized using random hexamer primers. One nanogram of the first strand cDNA was used for the PCR using the 5′-end primer 5′-AGCATCGAGTCGGCCTTGTTG-3′ and the gene-specific 3′-end primers used for the real-time RT–PCR.

For validation experiments using microarray, RNAs were isolated from the DLD-1 cells cultured in similar hypoxia (1% O_2) and normoxia (21% O_2) conditions. The RNAs were further processed according to the manufacturer's instructions Using the Agilent Human Gene Expression Array G4112F platform.

For the microarray analysis, for each of the total RNA preparations (from 1% and 21% O_2 conditions), 700 ng of total RNA was used for the labeling according to the manufacturer's instruction. The normalization was done at the sample preparation step. The following signal intensity processing was performed using GeneSpring (Agilent) with default parameters. The cut-offs used in this study was either 5-fold or 2.5-fold (Figure 2B). The experiments were repeated twice with the labeling dye exchanged.

For the comparison with the previous microarray studies, we retrieved the records from the GEO database (http://www.ncbi.nlm.nih.gov/geo/) [a: GDS2758-61 (7); b: GDS1209 (8); c: GDS2018 (6); d: GDS1779 (9), for the GEO accession numbers and references, respectively]. We examined the original papers and prepared the list of the 'hypoxia induced genes' from each of the datasets. Using these datasets, the overlap between the genes identified as 'hypoxia induced' by this study and the previous studies was examined.

RESULTS

Construction of a TSS-tag library

By combining the oligo-capping method with a massively parallel sequencing technology, Illumina GA sequencer, we developed a simple method to collect TSS information together with a quantitative analysis of the expression levels of the transcripts (digital expression profile) in an extremely high-throughput manner (Figure 1). First, the primer sequence necessary for the sequencing was directly introduced at the 5′-ends of capped transcripts by replacing the cap structure with a cap-replacing RNA oligo (11). Then, cDNA was synthesized using random hexamers, amplified with 15 cycles of PCR and directly introduced into the sequencer without cloning (for the detailed protocol, see Materials and Methods section). The 36-base long tags corresponding to the 5′-ends of transcripts were generated by the sequencer at the rate of 10–30 million TSS-tags per run. This simple procedure eliminates laborious cloning step and allows us to easily monitor the genome-wide positions of TSSs. Furthermore, the number of TSS-tags corresponds to the number of transcripts within the cell starting from that site, since each transcript has only one cap structure.

Validation of the TSS-tag library

We first validated whether the TSS-tags collected by this method correctly indicate the positions of the TSSs and whether the counts of the TSS-tags represent the expression levels of the transcripts *in vivo*. For this purpose, we constructed a TSS-tag library from human embryonic kidney 293 (HEK293) cells. In total, we generated 10 401 151 TSS-tags which were uniquely and perfectly (with no mismatch) mapped to the human genome (hg 18; UCSC Genome Browser). We compared the mapped position of the TSS-tags with 18 001 protein-coding RefSeq gene models. Genomic coordinates of exons and other information of the RefSeq transcripts are as described in hg18

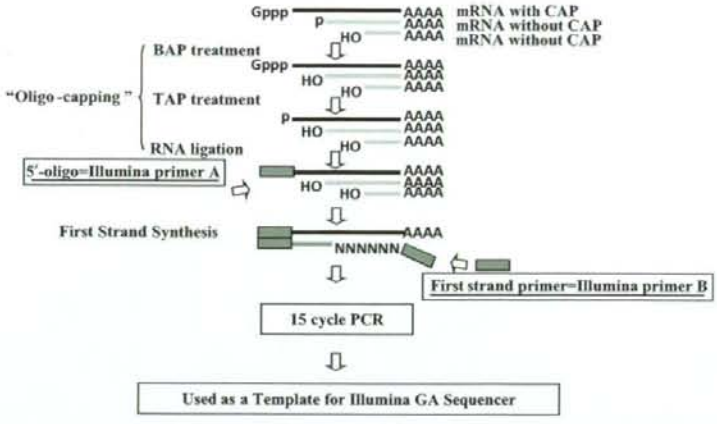

Figure 1. Scheme of 5′-end sequencing using the Illumina GA Sequencer. Adaptors containing necessary sequence for the Illumina GA sequencer are represented as grey boxes. For further information, see Supplementary Data. Gppp: cap structure. AAA: polyA.

as of UCSC Genome Browser (for the version information, see Materials and Methods section). As shown in Figure 2A, 8 647 513 (83%) of the TSS-tags were mapped within the RefSeq regions. Among them, 2 255 507 (26%) and 4 647 102 (54%) of the TSS-tags were mapped upstream and inside regions of the first exons, respectively. 739 319 (9%) of the TSS-tags were mapped to intronic regions of the RefSeq gene models, which may correspond to the TSSs of unknown alternative promoters, because there should be rare chance that they are derived from broken-down products of the mRNAs [for further discussion, see (15)]. Also, these numbers resemble the results from our previous analysis using 1.8 million 5′-ESTs (15). We observed no significant difference in the size of representative mRNAs between the TSS-library and the HEK293 oligo-cap cDNA library, which was constructed using random primers (data now shown).

Many of the TSS-tags which were mapped outside of the RefSeq regions overlapped with cDNAs in our cDNA collection (14). In particular, at least 1374 TSS-tag sites (mapped positions of the TSS-tags) overlapped with the 5′-ends of the 5′ESTs (also see Supplementary Figure 1 for further details). Of these, 80 TSS-tag sites overlapped with our completely sequenced cDNAs. For the latter cases, average length of the representative cDNAs was 2323 bp. Of these, 55 (70%) cDNAs were spliced and, in 53 (66%) cDNAs, the longest protein-coding region was less than 100 amino acids (300 bp). Therefore, many of those intergenic TSS-tag should represent so-called mRNA-like non-protein-coding transcripts (14,24,25). We further compared the TSS-tag sites with the 5′-end data from the RNA-Seq analysis (26) and the CAGE analysis (19), which have been the only two studies that produced comparable amount of the TSS information. Among the TSS-tag sites in our dataset, 1456 sites overlapped with the '5′ extension' data of the RNA-Seq analysis, of which 1105 sites also overlapped with the CAGE data. Although biological functions of many of those transcripts still remain elusive, the TSS-tags correctly represented the TSSs of previously identified transcripts.

We also wished to directly demonstrate the correct identification of the TSSs by luciferase reporter gene assays of the upstream regions of the TSS-tag sites and by real-time (quantitative) RT–PCR assays. In our previous study, we reported systematic luciferase assays in HEK293 cells (27). Among our TSS-tag dataset, luciferase data was available for the upstream regions (1 kb-upstream) of 359 TSS-tag sites. As shown in Figure 2B, distribution of the promoter activities for the 359 TSS-tag sites was clearly distinct from that of randomly isolated genomic fragments. Especially we observed clear promoter activities even for 14 TSS-tag sites with which no 5′ exons of the RefSeq gene models overlapped and for six additional TSS-tag sites which were located more than 50 kb apart from any of the RefSeq genes.

We then validated whether real-time RT–PCR primers targeted at the TSS-tags sites with no RefSeq gene support could detect transcripts, and to what extent the quantitative data are correlated with the TSS-tag counts. For the purpose of quantifications, we selected TSS-tag sites which overlapped with the 5′-ends of cDNA clones in our cDNA collection. We performed real-time RT–PCR using immediately downstream sequences of the TSS-tags for the 5′-end PCR primers (Figure 2C and D). We observed clear real-time RT–PCR signals for 80 TSS-tag sites within the RefSeq regions but outside of the 5′-ends of RefSeq gene models, and for 25 TSS-tag sites mapped outside of the RefSeq regions (overall success rate was 78%). We also performed independent oligo-cap RACE analysis and, for 21 TSS-tag sites (out of 25 cases attempted), we confirmed amplification of the cDNA fragments of the expected lengths. We further quantified the absolute expression levels of those 105 (80 + 25) TSS-tag sites by using the individually isolated and quantified cDNA plasmids as controls. As shown in Figure 2C, we observed that the correlation of the absolute expression

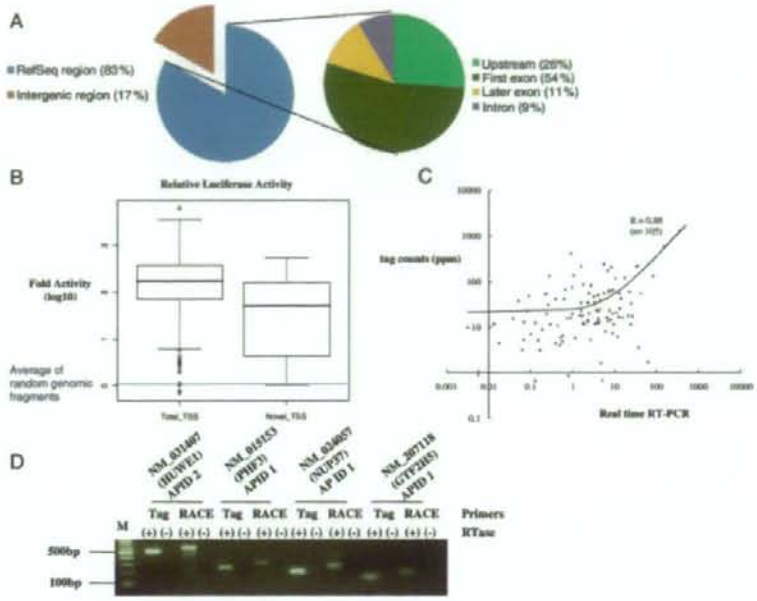

Figure 2. Validation analyses of the TSS-tag library. (**A**) Mapped positions of the TSS-tags relative to the RefSeq genes were evaluated. Population of the TSS-tags mapped at the corresponding positions indicated by the color bars in the margin is shown. The right circle graph shows the composition of the blue section in the left circle graph. (**B**) Distribution of the luciferase activities of the upstream 1 kb regions of the TSSs (n = 351; right). Luciferase activities of upstream regions of the TSS-tags that were not supported by any RefSeq gene models are calculated separately (n = 20; left). Luciferase activities were normalized against the average luciferase activity of randomly isolated 1 kb genomic fragments (n = 251). For further details, see the reference (27). (**C**) Correlation between the TSS-tag counts and the copy number estimated by real-time RT–PCR normalized by individual plasmids (n = 105). Each value is the average of three experiments. Sequences of the used primers and quantitative data are presented in Supplementary Table 10. R: correlation-coefficient calculated by linear regression. Note that, because the graph is written in log scale and the y intersect is not 0, the liner regression line is curved where the x value is small. (**D**) Examples of the real-time RT–PCR and independent oligo-cap RACE analyses. Experimental conditions are shown in the margin. For details, see Materials and methods section. For the primer, 'Tag' indicates the PCR primer targeted to the overlapping region of the TSS-tag and 'RACE' indicates the PCR primer targeted to the cap-replacing oligo. APID: alternative promoter ID. M: molecular marker.

levels calculated by the TSS-tag counts and the real-time RT–PCR are generally well-correlated, although we also observed deviations in some cases (also see Discussion section).

Based on these results, we concluded that our TSS-tag library analysis should be reliable and useful for identifying both the TSS positions and their corresponding expression levels.

Application of the TSS-tag library for the analysis of hypoxia responses in a colon cancer cell line

Taking advantage of this new method, we wished to reveal the dynamic nature of the human gene transcriptome in a focused cell type with particular environmental perturbations. We performed genome-wide analysis of the alterations in both promoter usage and expression levels of the transcripts invoked by hypoxia. In a human colon cancer cell line, DLD-1 cells, expression of a well known hypoxia-induced gene, VEGF, is induced under hypoxic culture condition as well as in xenografted tumor tissues *in vivo* (4). We cultured DLD-1 cells under hypoxic and normoxic conditions with and without transfection of siRNAs targeted to HIF1A or HIF2A. This experimental design is the same as the previous studies of other groups (5,7). We generated 15–19 million 36-base TSS-tags per condition (Table 1). A summary of the sequence quality is shown in Supplementary Table 1.

Overall mapping patterns were similar to the case of the HEK293 library (Table 1). For example, in the case of the 'hypoxia with non-targeted RNAi' library, 14 001 295 (73%) out of total 19 213 284 TSS-tags were mapped in the RefSeq regions. Of these, 4 310 405 (31%), 7 384 800 (53%) and 1 459 600 (10%) TSS-tags were mapped to the upstream, first exon and intron regions, respectively. Therefore, we estimated at least 84–94% of the TSS-tags represent the real TSSs in this case, too. For the purposes of the following analyses, the TSS-tags were further clustered into 500-bp bins to generate TSS clusters (TSCs) (15). In case of 'hypoxia with non-targeted RNAi' library, a total of 19 213 284 TSS-tags constituted 2 610 785 unique TSS-tags. These unique TSS-tags were further clustered into 1 428 455 TSCs. Of these TSCs,

Table 1. Statistics of the TSS-tags generated from DLD-1 cells

	Relative to RefSeq regions		Relative to exons of RefSeq gene models			
	#total mapped tag	#NM_associated tag (%)	Upstream (%)	First exon (%)	Other exon (%)	Intron (%)
Hypoxia non-targeted RNAi	19213284	14001295 (73)	4310405 (31)	7384800 (53)	846490 (6)	1459600 (10)
Hypoxia with HIF1A RNAi	17995370	13758453 (76)	4116100 (30)	6995301 (51)	1303571 (9)	1343481 (10)
Hypoxia with HIF2A RNAi	17047001	14304678 (84)	4547387 (32)	8045603 (56)	830696 (6)	880992 (6)
Normoxia with non-targeted RNAi	17878365	14194520 (79)	3850858 (27)	8449751 (60)	820989 (6)	1072922 (8)
Normoxia with HIF1A RNAi	15190726	12628363 (83)	3554553 (28)	7469575 (59)	822034 (7)	782201 (6)
Normoxia HIF2A RNAi	17175662	14117263 (82)	3702462 (26)	8810503 (62)	685561 (5)	918737 (7)
Total	104500408	83004572 (79)	24081765 (29)	47155533 (57)	5309341 (6)	6457933 (8)

Mapped positions of the TSS-tags were counted relative to RefSeq regions and relative to exons of RefSeq gene models, when mapped inside of the RefSeq regions.

477 936 (33%) were mapped to the RefSeq regions. The rest were mapped to intergenic regions (709 997; 50%) or to anti-sense regions of the RefSeq genes (240 522; 17%). Although the numbers of the TSCs, especially in the latter two TSC groups, are high, many of the TSS-tag counts within these TSC were usually one or two, possibly representing noise-level transcriptions in the cell (see Supplementary Figure 1; overlap with the 5′EST data is also shown there).

Genome-wide distribution of hypoxia responsive transcripts

We normalized TSS-tag counts of TSCs to tags per million (ppm). In order to avoid noise level signals and possible experimental errors, we focused on TSCs for which TSS-tag ppm increased by at least 5-fold, having more than 1 ppm TSS-tags. One ppm corresponds to 15–20 independent TSS-tags per TSC depending on the dataset. By the conservative criteria of >1 ppm and >5-fold, most of the intergenic TSCs were removed. Some of the transcripts of previously identified 'hypoxic responsive genes' were also removed. We tentatively employed these very conservative criteria, considering that this is the first analysis taking the TSS-tag approach. However, further detailed analyses and re-evaluation of the data should be necessary on very rarely expressed intergenic transcripts, although some of them might be the system noise of the transcription machinery. For the number of 'hypoxia-induced' TSCs with different parameters, see Supplementary Table 2.

In order to validate the calculated fold inductions, we performed real-time RT–PCR analysis. For this purpose, RNAs were independently isolated from the DLD-1 cells cultured in similar hypoxia (1% O_2) and normoxia (21% O_2) conditions. From this analysis, again, we observed that the expression information obtained using this method was well-correlated with the results obtained using real-time RT–PCR (Figure 3A). We then performed microarray analysis and compared the obtained data with the digital expression data using independently prepared RNAs. As shown in Figure 3B, the hypoxia responsive genes detected in microarrays were mostly detected so in the digital expression profiling, too. At the same time, we identified additional putative hypoxia responsive transcripts (TSSs) by the new approach possibly owing to the improved sensitivity and coverage of the analysis (see below).

We also compared the results of digital gene-expression data with the previous microarray studies. We first searched for the data focusing on hypoxia responses of human cells in GEO database (28). Then, we examined the original papers and retrieved a list of the genes which were identified as 'hypoxia responsive genes' in the corresponding study. We examined overlap of the 'hypoxia induced genes' identified from the previous studies and from this study. As shown in Figure 3C, 11 genes, which were reported as hypoxia responsive genes in at least two of the previous studies (6–9), were detected so in our tag-based approach.

Using the digital-expression data, we identified 9870 hypoxia-induced TSCs in total. Among them, 6366 (64%) were mapped to RefSeq regions on the sense strand (for the full list of the induced TSCs, see Supplementary Table 12). The rest were mapped to intergenic regions or anti-sense of the RefSeq regions. Gene-rich chromosomes 17 and 19 had the largest number of both genic and intergenic hypoxia-induced TSCs per genic and intergenic base of the chromosomes (Supplementary Table 3).

We found some genomic regions in which hypoxia-induced TSCs particularly clustered. We identified 54 genomic regions in which seven or more hypoxia-induced TSCs clustered in a 100-kb window (Figure 4A). In these regions, transcription was activated on hypoxia from both inter (Figure 4B) and intra (Figures 4C and 4D) genic regions. Furthermore, transcription activation in the genic regions shown in Figure 4C occurred regardless of their exon–intron structure (lower panel; also see Supplementary Figure 6). We also noticed distal regions of the chromosomes frequently have such 'hot regions' (Figure 4A; also see Supplementary Table 4). There might be cross-talk between transcription activation in these regions and chromatin remodeling accompanied by telomere elongation (29), which is a hallmark of cancer progression. We further searched for RefSeq regions with multiple induced TSCs. Of 6366 RefSeq regions that contained at least one hypoxia-induced TSC, 131 regions had five or more hypoxia-induced TSCs, reflecting

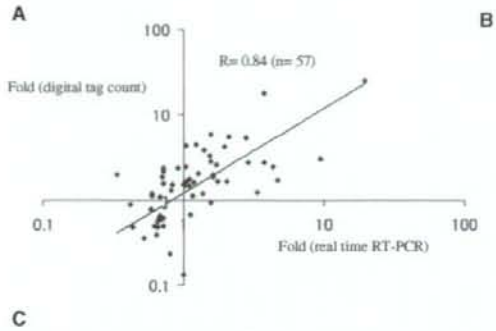

C

NM ID	definition	fold: hypoxia/normoxia (TSS-tag count)	fold: hypoxia/normoxia (realtime RT-PCR)	fold: hypoxia/normoxia (microarray in this study)	reference
NM_001124	adrenomedullin	12.5	6.1	4.1	a, b, d
NM_005165	fructose-bisphosphate aldolase C	25.2	19.2	5.7	a, c
NM_022073	egl nine homolog 3	3.0	62.0	9.1	a, d
NM_181054, NM_001530	hypoxia-inducible factor 1, alpha subunit	0.7	0.6	0.9	b, c
NM_000598, NM_001013398	insulin-like growth factor binding protein 3	5.1	2.0	1.5	a, b, c, d
NM_002317	lysyl oxidase preproprotein	5.4	2.1	2.4	a, b, c, d
NM_002318	lysyl oxidase-like 2 precursor	1.7	not amplified	1.2	a, d
NM_152878,NM_012323	transcription factor MAFF	4.4	not amplified	1.3	a, d
NM_006096	N-myc downstream regulated gene 1	18.8	20.5	7.5	a, d

Figure 3. Validation analyses of the fold induction. (**A**) Correlation between the fold changes observed using digital-expression information (vertical axis) and real-time RT–PCR (horizontal axis). In total, 57 genes out of 63 total glycolysis related genes, from which we obtained meaningful data, were used for the validation. Each value is the average of three experiments. Sequences of the used primers are shown in Supplementary Table 10. R: correlation-coefficient calculated by linear regression. (**B**) Validation experiments by the microarray analysis. Overlap of the microarray results and digital gene-expression profiling is shown in the bottom margin. The numbers in the parentheses indicate the number of genes induced by more than 1.5-fold (upper) and 2.5-fold (lower), although they were not detected as 'induced' by the criteria of 2.5-fold induction (upper) and 5-fold induction (lower). The statistical significance of the overlap by calculating hypergenometric distribution was $P < 5E{-}67$ for 2.5-fold change and $P < 3E{-}15$ for 5-fold change. (**C**) Comparison with data from previous studies. For the comparison with previous microarray studies, the overlap between the genes identified as 'hypoxia induced' by this study and the previous studies was evaluated. The 'hypoxia responsive genes' in the previous studies were as of those described in the corresponding papers.

the presence of multiple hypoxia-induced transcriptions start in a single gene. Collective transcriptional induction events as represented in Figure 4 should not be extremely rare.

Putative hypoxia responsive non-protein-coding transcripts

Among the 9870 hypoxia-induced TSCs, 3504 were located at least 50 kb away from any protein-coding genes in the same strand, thus they seemed driving non-protein-coding transcripts (25,30) (also see the legend for Supplementary Figure 1). We first searched for hypoxia-induced TSCs located in the proximal regions of previously reported intergenic miRNAs using miRBase (31). We found only two such cases; TSCs 7 kb upstream of hsa-mir-612 and 1 kb upstream of hsa-mir-675 were up-regulated by 18-fold and 8.7-fold, respectively. The latter TSC actually corresponded to the TSS of the H19 non-coding RNA, which is consistent with the recent finding that H19 RNA is induced in hepatocellular carcinoma cells upon hypoxia (32,33). Similarly, we examined overlap of the intergenic TSCs with another class of non-coding RNAs, namely snoRNAs (34). We searched snoRNABase (35) and identified five TSCs which were located within 2 kb of regions which contained altogether nine snoRNAs (see Supplementary Table 5A). Most of them were reported to be involved in maturation of ribosomal RNAs, indicating a possibility that general translational machinery might be altered in response to hypoxia.

Although TSS-tag numbers were low for most of the newly found hypoxia-induced intergenic putative non-protein coding transcripts (Supplementary Figure 1), there were still a number of cases where expression and induction levels were at similar levels to the above two cases (33 ppm and 175 ppm for hsa-mir-612 and 675, respectively). There were 220 TSCs with TSS-tags of >10 ppm (10 ppm corresponds about three copies per cell, assuming 3×10^5 transcripts within a cell; also see Supplementary Table 5B). Indeed, among those 220 TSCs, four overlapped with our completely sequenced cDNAs (Supplementary Table 5C), whose average length was 1974 bp and, for all of which the longest potential open reading frame was less than 150 amino acids (450 bp). It is also noteworthy that the number 220 is in the similar range of the number of hypoxia-induced protein coding genes (see below).

In order to further characterize these hypoxia-responsive TSCs, we analyzed the correlation of their fold inductions against the most proximal protein-coding